Photosynthetic and water transport strategies of plants along a tropical forest aridity gradient: a test of optimality theory

Corresponding author:

Huanyuan Zhang-Zheng, (0000-0003-4801-8771) (huanyuan.zhangzheng@gmail.com)

Author list:

Huanyuan Zhang-Zheng1, (0000-0003-4801-8771)

Yadvinder Malhi1, (0000-0002-3503-4783)

Agne Gvozdevaite1,

Theresa Peprah4,

Mickey Boakye3,

Kasia Ziemińska2, (0000-0001-7750-4758)

Stephen Adu-Bredu4,

Jesús Aguirre-Gutiérrez 1,(0000-0001-9190-3229)

David Sandoval 5,

Iain Colin Prentice 5, (0000-0002-1296-6764)

Imma Oliveras Menor1,2, (0000-0001-5345-2236)

1 Environmental Change Institute, School of Geography and the Environment, University of Oxford, Oxford, United Kingdom,

2 AMAP (Botanique et Modelisation de l'Architecture des Plantes et des Végétations), Université de Montpellier, IRD, CIRAD, CNRS, INRAE, Montpellier, France

3 Department of Environmental Science, Policy, and Management, University of California, Berkeley, CA, 94720, USA

4 Forestry Research Institute of Ghana, Council for Scientific and Industrial Research, Kumasi, Ghana

5 Georgina Mace Centre for the Living Planet, Department of Life Sciences, Imperial College London, Silwood Park Campus, Buckhurst Road, Ascot, SL5 7PY, UK

Word Count

Total word count for the main body of the text: 5426

Summary: 200

Introduction: 707

Materials and Methods: 2491

Results: 1029

Discussion: 999 (18.4% of total word count)

Number of figures:2 (all in colour)

Number of table: 1 (all in colour)

Supporting information is provided in another document.

Keywords

Optimality; photosynthesis; aridity; plant functional traits; plant hydraulics; xylem hydraulics

Summary

(1) The research conducted, including the rationale

The direct effect of aridity on photosynthetic and water-transport strategies is not easy to discern in global analyses because of large-scale correlations between precipitation and temperature. We analyze tree traits collected along an aridity gradient in Ghana, West Africa that shows little temperature variation, in an attempt to disentangle thermal and hydraulic influences on plant traits.

(2) Methods

Predictions derived from optimality theory on the variation of key plant traits along the aridity gradient are tested with field measurements.

(3) Results

Most photosynthetic traits show trends consistent with optimality-theory predictions, including higher photosynthetic capacity in the drier sites, and an association of higher photosynthetic capacity with greater respiration rates and greater water transport. Hydraulic traits show less consistency with theory or global-scale pattern, especially predictions based on xylem efficiency-safety tradeoff. Nonetheless, the link between photosynthesis and water transport still holds: species (predominantly deciduous species found in drier sites) with both higher sapwood-to-leaf area ratio (AS/AL) and potential hydraulic conductivity (Kp), implying higher transpiration, tend to have both higher photosynthetic capacity and lower leaf-internal CO_2.

(4) Conclusions

These results indicate that aridity is an independent driver of spatial patterns of photosynthetic traits, while plants show a diversity of water-transport strategies along the aridity gradient.

Plain language summary: Along an aridity gradient in Ghana, West-Africa, we used optimality theory to explain that aridity is an important driver of photosynthetic traits, independent of temperature. Toward drier sites, plants have higher photosynthetic capacities per leaf area but have fewer leaves. We also explain how plants arrange water transportation to support quicker

photosynthesis at drier sites. However, plants at the drier sites seem to have diverse combinations of hydraulic traits to satisfy the need for photosynthesis. We reported surprising data-theory inconsistency for some hydraulic traits along the aridity gradient where further research is needed.

Introduction

Three key photosynthetic processes are frequently considered when seeking to understand plants photosynthesis strategies: light availability and electron transport; aridity and water transport; and CO_2 concentration and carboxylation (Farquhar et al., 2001). Plants capacities in these photosynthetic processes vary considerably along environmental gradients (Wang *et al.*, 2017a; Bahar *et al.*, 2017; Yang *et al.*, 2019; Oliveras *et al.*, 2020). Recently, many efforts have been made to propose universal rules to explain worldwide plant photosynthetic strategies, frequently cited as 'optimality theories', which could serve as a basic theoretical framework for vegetation carbon modelling and enable quantitative predictions of key photosynthetic traits (Franklin *et al.*, 2020; Harrison *et al.*, 2021).

One of the main challenges confronting these universal rules is to explain the 'pure' effect of aridity on photosynthesis (Rogers *et al.*, 2017). Such challenges become particularly pressing in the context of climate change as greater atmospheric dryness (water vapour deficit, VPD) is predicted for most places (Neelin *et al.*, 2006; Grossiord *et al.*, 2020a; Bauman *et al.*, 2022), which may strongly influence photosynthesis and hence the carbon cycle (Canadell *et al.*, 2021). Although optimality theory has shown to successfully explain photosynthetic strategies on multiple scales (Peng *et al.*, 2020; Dong *et al.*, 2020; Harrison *et al.*, 2021), in previous studies, aridity was confounded with temperature, especially when VPD is used as a metric of aridity. Temperature is a stronger driver of photosynthesis than aridity (Smith *et al.*, 2019; Peng *et al.*, 2021), but few studies have tried to disentangle aridity from temperature (Grossiord *et al.*, 2020a). To date, the optimality-theoretical expectation for the impact of aridity on plant traits has not been summarized and tested. Most current earth systems models predict a negative relationship between photosynthesis (denoted by CO_2 assimilation rate per leaf area, A_{area}) and

VPD simply due to the closing of stomata without incorporating the dynamics of photosynthetic capacity (denoted by electron-transport capacity, J_{max25} and Rubisco carboxylation capacity standardized to 25 °C, V_{cmax25}) (Wang *et al.*, 2017a; Green *et al.*, 2020). On the contrary, a study focusing on Amazonia argued that photosynthetic capacity is higher for leaves grown in dry season which counteracts the reduced stomatal conductivity, leading to higher photosynthesis under drier climates (Restrepo-Coupe *et al.*, 2013; Green *et al.*, 2020). Globally higher V_{cmax25} was indeed found for plants grown in drier sites (Cernusak *et al.*, 2011; Peng *et al.*, 2021; Dong *et al.*, 2022). Under experimental conditions, plants grown under low VPD show no difference in CO_2 assimilation to plants grown under normal VPD (Cunningham, 2005).

Despite the need of incorporating the dynamics of photosynthetic capacity in models, the stand-alone effect of aridity on photosynthesis adaptation still remains unclear. There are two particular challenges. First, aridity can be confounded with temperature on a large spatial scale or temporal scale (Grossiord *et al.*, 2020a). Second, optimality theory predicted higher V_{cmax} and A_{area} under higher VPD (Smith *et al.*, 2019) but it is unclear how plants in drier environments arrange water transportation through xylem to support higher $A_{area.}$ A comprehensive theoretical framework is lacking to incorporate the effect of VPD on all leaf-level photosynthesis processes (light, water and CO_2) with consideration of water delivery to leaves (Mencuccini *et al.*, 2019a).

Here, we examine a dataset of detailed traits measurements along an aridity gradient in West African forests to disentangle the effect of aridity on photosynthesis from temperature and to explain the effect with optimality theory. The key questions we address are: (1) do plants in drier environments have higher photosynthesis rates and how do aridity and photosynthesis interact? (2) If photosynthetic rates are higher in arid environments, as predicted by optimality theory, how do plants arrange greater water transportation under greater atmospheric dryness? To answer these questions, we adopted a theory-data comparison approach where we first review the expectation of recent 'universal' theories and deduced 16 testable predictions (some of which have previously been tested but with confounding results). We then examined the consistency between each prediction and field measurement along the aridity gradient (Table 1). Consistency would give field-observed patterns a mechanistic explanation and reinforce the stand-alone impact of aridity on the corresponding trait, while inconsistency would imply weakness of the

theory and the possible effect of other environmental factors (like soil properties). Before closing the paper, we summarize the consistency and inconsistency with an integrated theoretical framework to address the 'pure' effect of aridity on photosynthesis.

Review of Optimality theory

'Optimality theory' was developed recently with the assumption that plants can optimize photosynthesis and minimize maintenance costs according to their living environments, which provides a universal explanation of the variation of photosynthetic strategies under different growing environments (Prentice *et al.*, 2014; Sperry *et al.*, 2017; Wang *et al.*, 2017b; Mencuccini *et al.*, 2019a; Stocker *et al.*, 2020; Xu *et al.*, 2021). Although the above-cited studies have tested the theories on global scales and along elevation gradients, discussion and validation of these theories along aridity gradients, are still lacking. Therefore, we first review the implication of such theories on plants photosynthetic strategies along aridity gradients.

As predicted by the 'least-cost hypothesis' (Wright *et al.*, 2001, 2003; Medlyn *et al.*, 2011; Prentice *et al.*, 2014), plants in dry climates maximize the carbon return per molecule of water by keeping stomata relatively closed. Thus, in drier sites, plants are expected to have a lower leaf internal-to-external CO_2 ratio (c_i/c_a) and lower stomatal conductance (g_s). The 'coordination hypothesis' (Beerling & Quick, 1995; Maire *et al.*, 2012; Walker *et al.*, 2014) assumes equilibrium between Rubisco-limited photosynthesis rates (A_C) (depending on V_{cmax25} and c_i) and electron transport-limited photosynthesis rates (A_J) (depending on J_{max25} and leaf absorbed photosynthetic photon flux density, PPFD) (see the quantitative expression in (Wang *et al.*, 2017b; Smith *et al.*, 2019; Stocker *et al.*, 2020)). To maintain such an equilibrium, plants in drier sites are expected to have larger V_{cmax25} to compensate for the lower c_i. Otherwise, A_C would be lower than A_J resulting in the waste of light (PPFD). To sum up, lower c_i but higher V_{cmax25} is expected toward drier sites if J_{max25} stays constant (in which case A_J would be slightly lower due to smaller c_i).

In reality, toward drier sites, it is common to see higher leaf-absorbed photosynthetic photon flux density (I_{abs}) because of less cloud cover and more open canopies. Considering an additional optimality criterion that J_{max25} is acclimated to I_{abs} (Smith *et al.*, 2019), supported by multiple

153 experiments (Björkman, 1981; Ögren, 1993), we would expect higher J_{max25} and A_J in drier sites,
154 which further encourages higher V_{cmax25} (see above paragraph). Higher J_{max25} would give rise to
155 higher A_J, implying higher A_C following the 'coordination hypothesis'. All the above would
156 lead to high leaf photosynthetic protein cost in dry sites, hence high leaf dark respiration (Rd),
157 and high transpiration stream maintenance cost (see below for transpiration), hence higher stem
158 respiration per leaf area (R_{stem_leaf}) (Prentice *et al.*, 2014). Note that R_{stem_leaf} is stem respiration
159 per leaf area, different from the commonly reported stem respiration per stem area (R_{stem_stem}).
160 Some of the above predictions have been seen on global scale; for example, higher R_d has been
161 found in drier sites (Wright *et al.*, 2001; Atkin *et al.*, 2015) and higher assimilation rate has been
162 reported from drier sites (Cernusak *et al.*, 2011; Maire *et al.*, 2015; Peng *et al.*, 2021; Dong *et al.*,
163 2022).

164 It is worth noting that V_{cmax25}, g_s and c_i in this paper are discussed as an overall value for a forest
165 stand, disregarding diurnal variation and intraspecific variation (Stangl *et al.*, 2019; Han *et al.*,
166 2022). For instantaneous measurements, there is a positive correlation between A_{sat} (light-
167 saturated assimilation rate at 400 ppm), V_{cmax25}, g_s and c_i (Wright et al., 2003; Fig.2 in Prentice et
168 al., 2014), instead of the opposite trend of V_{cmax25} and c_i/c_a discussed above regarding spatial
169 variation only.

170 Photosynthesis strategies predicted by the optimality theory above can be linked with stem
171 xylem water transportation strategies via stomatal behaviour, as given by Fick's law,

172 $$g_s = A_{area} / (ca - ci) \quad (1)$$

173 Where g_s is stomatal conductance (umol CO_2 m^{-2} s^{-1}), A_{area} is CO_2 assimilation rate per leaf area
174 (umol CO_2 m^{-2} s^{-1}), and leaf internal (ci, ppm) and external (ca, ppm) CO_2 concentration

175 We focus on daytime conditions that produce maximum rates of transpiration and photosynthesis,
176 when water loss through stomata must equal water transport through xylem (assuming no change
177 of stored water) (Brodribb *et al.*, 2002; Xu *et al.*, 2021):

178 $$E/A_L = 1.6\ gs\ VPDla / Patm = Ks\ \Delta\Psi max\ A_S/A_L\ / h \quad (2)$$

Where E/A_L is water transpired per leaf area surface (mol m^{-2} s^{-1}), VPDla is leaf-to-air VPD, Patm is atmospheric pressure (Mpa), Ks is sapwood-specific hydraulic conductivity (mol $m^{-1}s^{-1}$ MPa^{-1}); A_S/A_L is the ratio of sapwood to leaf area (m^2m^{-2}), $\Delta\Psi$max is the maximum decrease in water potential from soil to leaves (MPa), h is the transpiration stream path length (m), roughly equivalent to plant height, $1.6 * g_s * VPD_{la} / P_{atm}$ denotes 'water loss through stomata', and Ks $\Delta\Psi_{max}$ A_S/A_L / h denotes water transport through xylem.

Combining the above two equations we obtain a link between water transportation and photosynthesis:

$$K_S \Delta\Psi max A_S/A_L / h = 1.6 VPDla A_{area} / (ca - ci) /Patm = E/A_L \quad (3)$$

Which could be rearranged to focus on carbon gain:

$$A_{area} = K_S \Delta\Psi max A_S/A_L / h /1.6 /VPDla * (ca - ci) * Patm \quad (4)$$

Note that Equation 3 was presented on whole-tree level but was tested using shoot level traits (Xu *et al.*, 2021), as well as in this study. Here we disregard diurnal or seasonal variation. Relationships could be very different at other time scales (Mencuccini *et al.*, 2019a).

In drier sites with higher VPD, despite smaller g_s, there should inevitably be a larger E/A_L (Granier *et al.*, 1996) and more negative $\Delta\Psi_{max}$ (Gleason *et al.*, 2013); therefore smaller maximum tree height (Equation 3), and more negative turgor loss point (TLP, Mpa) in drier sites to increase hydraulic resistance (note that TLP must be more negative than $\Delta\Psi$max) (Ryan & Yoder, 1997; Bartlett *et al.*, 2012). Equation 3 implies that in drier sites with high VPD, plants require a larger A_S/A_L and/or larger Ks in order to support the same amount of photosynthesis with enhanced transpiration. Following the xylem safety–efficiency trade-off (Manzoni *et al.*, 2013; Gleason *et al.*, 2016; Bittencourt *et al.*, 2016; Grossiord *et al.*, 2020b), plants at drier sites would be expected to have lower hydraulic conductivity (K_S). Although arguments against this trade-off exist (Gleason *et al.*, 2016; Körner, 2019; Liu *et al.*, 2021), here we present testable hypotheses expected by the trade-off. At dry sites, lower hydraulic conductivity is often associated with smaller vessel diameter, higher vessel density and higher wood density (Poorter *et al.*, 2010; Schuldt *et al.*, 2013; Hoeber *et al.*, 2014). Such patterns have been observed along

206 an Australian aridity gradient (Gleason *et al.*, 2013; Pfautsch *et al.*, 2016), but no effect of aridity
207 on vessel diameter was reported elsewhere (Olson & Rosell, 2013; Olson *et al.*, 2014). Plants in
208 drier sites should have increased hydraulic safety - more negative TLP and more negative P50
209 (Hacke *et al.*, 2001; Martínez-Vilalta *et al.*, 2009; Gleason *et al.*, 2013; Togashi *et al.*, 2015; Liu
210 *et al.*, 2019; López *et al.*, 2021). In short, toward drier sites, we would expect to see, higher
211 A_S/A_L and more negative TLP. The safety-efficiency trade-off implies lower K_S, smaller vessel
212 diameter, higher vessel density and higher wood density.

213 The trade-off between Ks and A_S/A_L is also embedded in the variance of traits in equation 3. K_S
214 and A_S/A_L could vary by two orders of magnitude (100-fold variation) (Mencuccini *et al.*, 2019b)
215 on a global scale, while ci/ca and A_{area} vary much less (ci/ca: 2 fold; A_{area}: 10 fold) (Wright *et al.*,
216 2004; Wang *et al.*, 2017b). This leads to a trade-off between K_S and A_S/A_L (i.e. K_S x A_S/A_L
217 should vary less than either of them). However, given that there are also variations of ci/ca, A_{area},
218 h and $\Delta\Psi max$, it is possible that different species range along a spectrum from high A_{area} and
219 E/A_L to low A_{area} and E/A_L while always satisfying equation 3 (Prentice *et al.*, 2014).

220 In short, the above review leads to hypotheses that plants in drier (normally also brighter) sites
221 tend to develop a photosynthesis strategy with less stomatal conductance and lower ci, stronger
222 photosynthetic capacities (larger V_{cmax25}, J_{max25} and A_{area}) with more maintenance cost (higher Rd
223 and Rs) and larger transpiration per leaf area which the water transport system would adjust to
224 with higher A_S/A_L, lower Ks, lower tree height and more negative TLP. We break the above
225 prediction down into 16 testable hypotheses (Table 1) and test each of them along a forest aridity
226 gradient.

227

228 Materials and Methods

229 Study sites - the aridity gradient

230 This study presents and analyses physiological traits data collected from seven one-hectare forest
231 and savanna plots distributed along a wet-dry gradient across three sites, Ankasa (ANK, moist

rainforest), Bobiri (BOB, semi-deciduous forest) and Kogyae (KOG, dry forest and mesic savanna), in Ghana, West Africa (Figure S1, S2) (Moore *et al.*, 2018; Oliveras *et al.*, 2020), as part of the Global Ecosystem Monitoring (GEM) network (Malhi *et al.*, 2021). These sites share very similar mean annual temperature but span a steep gradient of aridity (Figure 1), which provided a "natural laboratory" to disentangle the hydraulic aspect of plant traits variation from temperature. Light increase toward drier sites (Table S 1). There is no seasonal variation in temperature. Two rain seasons (Figure S9 S10) in all study sites occurred in similar months but the total amount of precipitation increases from dry to wet site. Latitude, longitude, number of species and more information are provided in Table S 1.

Although one-hectare plots (e.g. BOB-02) within the same site (e.g. BOB) share very similar air temperature and precipitation, they can differ in terms of belowground water supply due to small-scale variations in soil properties and topography (Table S 1). Along the aridity gradient, there are also variations in soil and vegetation type, with vegetation seasonality and deciduousness increasing considerably towards drier sites. More information about the soil properties and climate of all three sites can be found in (Domingues *et al.*, 2010; Chiti *et al.*, 2010; Moore *et al.*, 2018). Moreover, the swampy rainforest (ANK03) is partly inundated during the wet season but not ANK01, which is located on a hill and never inundated. From KOG02 (dry forest), KOG04 to KOG05 (savanna), forest plots become more deciduous with a smaller number of trees(Table S 1). Nonetheless, many species are 'semi-decideous' which shed only part of the canopy in the dry season. Within any site, there are many common species between plots but species composition (e.g., top five abundant species) could still be very different. There are almost no common abundant species between the three sites (ANK, BOB and KOG).

Aridity indices and soil moisture

Although the Introduction focuses on VPD, we only have one meteorological station at each site which could not tell VPD difference between plots. We thus provide other indices of aridity. At site scales, we provide Maximum Cumulative Water Deficit (MCWD) and Aridity index (the ratio of annual potential evapotranspiration (PET) to mean annual precipitation (MAP)). At plot scale, we reported not only measured surface (12 cm depth) soil volumetric water content, but

also hydraulic simulations on plot scales with SPLASH v2.0 (Sandoval & Prentice, 2020). This model requires three sets of input data: (1) field observed climate data at site scale during 2011-2016 (2) soil properties measured following the RAINFOR protocols (Quesada *et al.*, 2010); (3) terrain data: root zone was assumed 2m, while upslope drainage area, slope inclination and orientation were extracted from a global dataset (Yamazaki *et al.*, 2019). We considered two model output indices: the relative soil moisture saturation (Θ), defined as the volumetric water content (θ) normalized by the volumetric water content at saturation (θ_{SAT}); a vegetation water stress index (α), estimated as the ratio of annual actual evapotranspiration (AET) to PET. There are more indices shown in Table S 1 and Table S 2.

Functional trait data measurements

Leaf traits field campaigns were conducted using a standardized protocol between October 2014 and September 2016 in all plots (Oliveras *et al.*, 2020), covering both dry and wet seasons for some traits (see Appendix 1 for sampling protocol). We selected species that contributed to up to 80% of the basal area of each plot and sampled the three largest individuals for each species. From each selected individual, we sampled a sun and a shade branch, and from each branch, we used three leaves and three wood segments to measure leaf and wood traits, respectively. Only sunlit samples were used in this analysis because temperature and light of the shade leaves vary considerably from plot to plot which dilutes the focus on the effect of aridity. The specific number of samples and number of individuals sampled could be found in Table S 1, Figure 1 and Figure S 3.

Wood anatomical traits were analysed in the cross-sectional area of one twig of the sun branch per individual (i.e. three replicates per species) (protocol in Appendix 1). Equation 3 could be interpreted on whole-plant level or shoot level. However, whole-plant traits are challenging to measure and this study is conducted on shoot level. We used K_P (potential sapwood-specific hydraulic conductivity) as a proxy of K_S. K_P was calculated from vessel density and vessel diameter following (Poorter *et al.*, 2010). Nonetheless, K_P and K_S may decoupled as not entire sapwwod conducts water (Jacobsen *et al.*, 2018). We used twig A_S/A_L as a proxy of whole tree

288 A_S/A_L. We used plant stature (H_{max}) as a proxy of path length (h). Although H_{max} omits
289 information on root length and multi-layer canopy structure, the proxy would satisfy the need for
290 hypothesis testing in the study region but should be used with caution in future modelling studies.

291 We calculated stem respiration per leaf area (Rs_leaf) instead of the commonly presented
292 Rs_stem, as a 'maintenance cost of photosynthesis' (See Appendix 1) (Prentice *et al.*, 2014). To
293 our knowledge, Rs_leaf has not previously been presented with in-situ data in the literature. Here
294 we argue the importance to understand stem respiration from per leaf area perspectives because
295 (1) looking at plans from an integrated view, a leaf does not exists alone but exists associated
296 with a full hydraulic system and Rs_leaf integrates the maintenance cost of this full continuum
297 (Prentice *et al.*, 2014) (2) consistency with other photosynthetic traits which were reported per
298 leaf area.

299 All trait data reported in this study were field-measured except for wood density, which was
300 obtained from a global species database (Zanne *et al.*, 2009). Net primary productivity was
301 retrieved from (Moore *et al.*, 2018). Global scale sapwood-to-leaf-area ratio in Figure S6 and S4
302 are sourced from (Mencuccini *et al.*, 2019b). Global scale vessel diameter used in Figure S4 is
303 sourced from (Choat *et al.*, 2012). Multiple sources of data were joined using species names.

304 ## Statistical analysis

305 Hypotheses 1-14 (Table 1) were tested by significant differences between wet and dry plots.
306 Principal component analysis (PCA) and standardized major axis regression are used to
307 understand the relationship between Ks, A_S/A_L and photosynthesis traits (Hypothesis 15-16).

308 We performed a plot-to-plot comparison in answering Hypotheses 1 to 14 as follows: (1) We
309 visually inspected histograms of each trait and transformations to normal distribution were
310 applied if necessary. (2) Outliers were checked with the R package *outliers::scores*, interquartile
311 range method (IQR) with threshold 1.5 (Komsta, 2011). Extreme values were kept when we
312 were sure that they were devoid of errors (3) Community-weighted means were calculated based
313 on the basal area of each species. Standard error was calculated with the same weights
314 (Madansky & Alexander, 2017). (4) Significance of differences in plot-to-plot community-

weighted means were then tested with Tukey's one-way ANOVA using *lm()*, *glht*(), and *cld*() from *multcomp* package (Hothorn *et al.*, 2008), using basal area as weights. In testing Hypotheses 1-14, a hypothesis was accepted if KOG (dry region) was significantly different to ANK (wet region) while BOB (middle aridity) sat in between (Figure 1). (5) Variance partitioning was done with *vegan::varpart()*, following redundancy analysis ordination (RDA) method with the expression: *varpart* (Trait, ~ Plot, ~ Species, data = Trait). Variance partitioning reveals whether the change of traits along the aridity gradient was driven by intraspecific or interspecific variation. Note that plots within one site share common species (e.g. ANK01 to ANK03), but species composition is very different between sites (e.g. ANK01 to KOG02). Variance partitioning is also used to diagnose whether the intra-specific variation or measurement errors are overwhelming. To double-check the impact of intraspecific variation, we recalculated a community-weighted mean by assuming that the same species share the same value of trait (i.e. remove intraspecific variation) and extrapolated traits value to forest plots without trait measurements (Appendix 5)

For hypothesis 16, we applied Principal Component Analysis (PCA) with *FactoMineR::PCA*() (Lê *et al.*, 2008). A_{sat}, K_P, A_S/A_L and V_{cmax25} were log10 transformed. We avoided standardization by disabling 'scale.unit' in function PCA() so that the variance of a trait was reflected by the length of an arrow in Figure 2. For hypothesis 15, the slopes and significance of correlation were calculated by Standard Major Axis Regression (*function smatr::sma*()), commonly used for summarizing the relationship between two plant traits (Wright *et al.*, 2005; Warton *et al.*, 2012) as it considers uncertainties of both axes. All analyses were done at the species level (i.e. each point in Figure 2 represents a species) to compare with other studies and join among datasets. Hypothesis 15 was also tested at the global scale because Ks was reported to negatively correlate with A_S/A_L but there is no report on the global correlation between Kp and A_S/A_L (Appendix 4).

Results

Aridity gradient

The values of the aridity index (PET/MAP) (site scale) reveal a clear aridity gradient from ANK (moist rainforest site) to BOB (mid) and KOG (dry) (Table S 2). The same order could be arrived at with VPD or maximum cumulative water deficit (MCWD).

On the other hand, the simulations of relative soil moisture saturation (Θ) and vegetation water stress index (α) (plot scale) show that plants at BOB were the least soil moisture stressed, followed by ANK and KOG. BOB-02 has the highest values in these two metrics, different to surface soil moisture (Figure 1). The model reports the highest runoff at ANK-03, capturing to some degree the seasonal flooding, as also observed in the field. The different patterns of Θ (or α) to aridity index along the aridity gradient are caused by the soil characteristics which in turn define water holding capacity and hydraulic conductivity; for example, the plots in BOB are atmospherically drier (higher PET/MAP) than in ANK but they could hold more water (higher Θ). Especially in BOB-02, the infiltration rate is strongly reduced by low soil saturated hydraulic conductivity (60 mm/hr, less than half of ANK plots), and hence water can stay more time in the root zone while percolating. This acts as a buffer against the evaporative demand, maintaining water availability during dry months. The hydrological modelling outputs also match with field observation of surface soil volumetric water content (Figure 1) and plot vegetation characteristics (Figure 1, S2). For presentation (Figure 1), we rank sites by MCWD and then plots within sites by volumetric water content.

The effect of aridity on traits

From a photosynthesis perspective, along the aridity gradient, we see consistency between theoretical prediction and field measurements (Table 1) for all traits: toward drier site, ci/ca decreases (0.85 to 0.71), V_{cmax25} increases (21.58 to 46.48 umol CO_2 m^{-2} s^{-1}), J_{max25} increases (38.48 to 91.44 umol CO_2 m^{-2} s^{-1}), R_d increases (1.66 to 2.41 umol CO_2 m^{-2} s^{-1}), R_{stem_leaf} increases (0.03 to 0.12 umol CO_2 m^{-2} s^{-1}), A_{sat} increases (4.56 to 7.72 umol CO_2 m^{-2} s^{-1}) and A_{max} increases (15.88 to 22.86 umol CO_2 m^{-2} s^{-1}). The trends of all photosynthetic traits are

successfully predicted by theories based on VPD alone (but note that soil moisture and other aridity indices covary with VPD). As leaf economy traits (Figure S3) and soil nutrients (Table S1) overall do not have a clear trend along the gradient, considering nutrient cycling does not seem to aid the prediction of variation of photosynthetic traits along the aridity gradient.

From a water transpiration perspective, the hypotheses are consistent with field measurements for leaf traits. A_S/A_L is higher in drier sites (359.62 to 901.66 cm^2 m^{-2}) and TLP is more negative in drier sites (-1.33 to -1.63 Mpa). However, less consistency is found between theoretical expectations and field measurements for xylem-related traits. Along the aridity gradient, there is an increasing trend of field K_P toward drier sites (from 28.62 to 59.29 kg m-1 Mpa^{-1} s^{-1}), against the xylem safety-efficiency trade-off. Considering that K_P is calculated from vessel diameter and density. Behind the above trend, vessel diameter also contradict the hypotheses. Vessel diameter does not change along the aridity gradient, while vessel density increased toward drier sites (from 44.57 to 69.69 mm^{-2}). The theory expects lower K_P and hence higher wood density toward drier sites, but the drier plots (KOG04, KOG05) have higher K_P, higher twig density and higher wood density than the wettest site (ANK03). Meanwhile we also find K_P negatively correlates with twig density on species scales (a Simpson's paradox, see Appendix 4). ANK-01 has very high wood density and twig density which breaks the increasing trend formed by other plots. H_{max} decreases from wet to dry sites as expected.

Using variance partitioning, we find that the plot-to-plot trends of all traits are dominated by inter-specific rather than intra-specific variation (i.e., components [a] are smaller than [b] in Appendix 5) (i.e. the change of species composition). The analogous patterns between twig and wood density along the aridity gradient also support species turnover since twig density was field measured and wood density was parsed from a global database by species (Zanne *et al.*, 2009). Nonetheless, variance induced by 'not changing species and not changing plot' or simply measurement errors (component [d]) were large for many traits: accounting for 95% of turgor loss point variance, followed by V_{cmax25} (74%) and J_{max25} (66%).

The coordination between photosynthesis and water transportation

Data from our West African aridity gradient reveal a weak positive correlation between Kp and A_S/A_L, contradictory to Hypothesis 15, and inconsistent with the negative correlation that emerged on global scales (Appendix 4). A_S/A_L for the Ghanaian aridity gradient is higher than the pantropical average. For hypothesis 16, we further explore the link between A_S/A_L, Kp and photosynthetic trait. Species with both high A_S/A_L and Kp tend to have higher V_{cmax25} and lower ci/ca. Such species tend to be deciduous and appear more in drier plots (Figure 2). There is a larger variance of hydraulic traits compared to photosynthetic traits. The pattern is consistent if we redo the above PCA with Asat instead of V_{cmax25} (Appendix 4). This finding supports hypothesis 16 (Table 1) as well as equation 3.

Discussion

The trend of traits along the aridity gradient

Although most hypotheses (Table 1) have been tested with spatially varying aridity at multiple scales (Harrison *et al.*, 2021), testing them along the Ghana aridity gradient helps to scrutinize the pattern in the absence of temperature variation. The patterns of all photosynthetic traits measured along the aridity gradient (ci/ca, J_{max25}, V_{cmax25}, R_d, R_{stem_leaf}, A_{sat}, A_{max}, namely hypotheses 1-7) are consistent with the theoretical expectations, which underscores that aridity is a direct and critical driver of photosynthetic traits in absence of confounding effect with temperature. The increase of photosynthetic capacity towards drier sites is useful in explaining multiple previous observations: (1) Savanna has higher A_{sat} and A_{max} than wet evergreen forest (Gvozdevaite, 2018; Oliveras *et al.*, 2020) (2) In the tropics, drier sites are brighter and warmer where higher photosynthetic capacity imply higher actual CO_2 assimilation per leaf area. This explains the previous finding that woody savanna has sparse canopy but similar net primary productivity to wet evergreen forest (Figure 1) (Moore *et al.*, 2018). As leaf area index decreases toward dry sites and photosynthesis rate increases, the mid-aridity site could be the most productive (Moore *et al.*, 2018). (3) For wet Amazonia forests, leaves flushed in dry season have higher photosynthetic capacities which increase forest productivity (Wu *et al.*, 2020; Green *et al.*, 2020).

From a water transportation perspective, forests in drier sites have higher TLP, lower H_{max} and higher A_S/A_L, in support of a greater mid-day transpiration stream (agreed with hypotheses 8-10). However, we found slightly higher K_P toward drier sites inconsistent with hypotheses derived from the safety-efficiency trade-off. First, it could be associated with the difference between K_P and Ks –vessels embolized in drier sites are not dected by anatomical images and not entire sapwood conducts water (Jacobsen *et al.*, 2018). It is possible that the trade-off work well only for single-species studies (Pritzkow *et al.*, 2020) and become weak on large scales and across species (Gleason *et al.*, 2016; Grossiord *et al.*, 2020b). Much higher deciduousness in KOG (dry site) than in the wet sites may play a role as higher hydraulic efficiency was observed from deciduous species or more deciduous forests (Choat *et al.*, 2005; Chen *et al.*, 2008; Liu *et al.*, 2021) as they need less hydraulic safety (Körner, 2019). Furthermore, the increase of K_P along the aridity gradient is not inconsistent with previous global analysis: First, the trade-off is not strong (or not a strict 1:1) and per given hydraulic safety, a wide range of efficiency was observed in a global dataset (Gleason *et al.*, 2016). Second, for environments with wet soils and dry atmosphere, high hydraulic efficiency was observed which reduce xylem water potentials and thus avoid harmful tension in the first place (Gleason *et al.*, 2013). We reported a negative correlation between A_S/A_L and Kp at global scales but a positive correlation along the aridity gradient (Appendix 4). One of the reasons for these contrasting opposite correlations may lie in a geographical sampling bias – the global dataset with scarce data points from West Africa compared with the Ghanaian dataset. The other possibility could be a confounding effect by temperature or vegetation type at the global scale; for example, a negative correlation between A_S/A_L and Ks was reported globally (Mencuccini *et al.*, 2019b) and on continental (Australia) scales (Gleason *et al.*, 2012), but an insignificant correlation was also reported for tropical forest stands on local scales without varying temperature (Poorter *et al.*, 2010; Schuldt *et al.*, 2013; Hoeber *et al.*, 2014).

By assuming that traits with a clear and strong trend along the aridity gradient are more tightly bound with aridity (Figure 1), ci/ca (stomata behaviour), TLP (drought tolerance) and A_S/A_L (water delivery) are found to be the most aridity-driven traits. The runners-up are R_d, R_{stem_leaf}, J_{max25}, and V_{cmax25}, which was thought acclimated to ci/ca and light intensity (Wang *et al.*, 2017b). Although ci/ca, V_{cmax25}, K_P and A_S/A_L all vary from wet to dry sites, we further illustrate that,

surprisingly, it is photosynthetic traits instead of hydraulic traits that contrast species from wet to dry sites (also from evergreen to deciduous) (Figure 2). Given that large photosynthetic traits variation from wet to dry plot was induced by species turnover (Appendix 5), our studies hint that facing a drier climate, if allowed time, West African forests photosynthesis could adapt to a drier climate by changing species abundance with possibly more deciduousness and higher photosynthesis capacity albeit less stomatal openness (Aguirre-Gutiérrez *et al.*, 2019). Without consideration of the positive effect of aridity on photosynthetic capacity, models could underestimate forest productivity under future drier climates.

Combining photosynthesis and hydraulic hypotheses

Overall, optimality theory can well explain plant photosynthesis strategies along the aridity gradient and we also expand the theory to consider water transportation. Namely, species in drier sites (with more deciduousness) tend to develop a photosynthesis strategy with less stomata openness (ci/ca), stronger photosynthetic capacities (J_{max25} and V_{cmax25}) with more maintenance cost (higher R_d and R_{stem_leaf}), quicker photosynthesis rate (A_{sat}) and larger maximum transpiration per leaf area, supported by larger K_P and larger A_S/A_L. The product of A_S/A_L and K_P is a proxy of water delivery per leaf area, which was previously found well correlated with proxies of photosynthesis rate: Asat (Santiago *et al.*, 2004), the quantum yield of electron transport (Brodribb & Feild, 2000) and electron transfer rate (Brodribb *et al.*, 2002), consistent with this study (Figure 2). The large variance of wood traits (way larger than leaf photosynthetic traits) (Mencuccini *et al.*, 2019b) (Figure 2), hints that plants might have a wide range of choices of traits combinations to provide adequate water transportation (Sperry *et al.*, 2002; Prentice *et al.*, 2014) in drier sites to support faster photosynthesis. The study also highlights the central role of A_S/A_L, or LAI on forest stand scale, or deciduousness on temporal scale, in controlling water relations. Further investigations into xylem functioning are required to further understand how larger water transportation was achieved in drier sites. Although we successfully predicted plants photosynthesis strategies along the aridity gradient (hypothesis 1-7) based solely on VPD without mentioning soil nutrients nor soil moisture, the theoretical deduction implicitly assumes that plants in our study site have adequate access to soil nutrient and belowground water. Further, since soil moisture and VPD co-vary along the aridity gradient and both can cause stomata

483 closure (Rodriguez-Dominguez & Brodribb, 2020), their effects are confounded in this study.
484 Thus caveats should be given to model the effect of aridity using only VPD, especially since soil
485 moisture may be playing a role at other temporal scales (e.g., daily) (Liu *et al.*, 2020; Fu *et al.*,
486 2022) or under extreme soil drought (Sperry *et al.*, 2002).

487 Conclusion

488 Along the aridity gradient, we find that at drier and brighter sites with more decideousness,
489 species tend to have higher V_{cmax25} and lower ci/ca with both higher A_S/A_L and K_P (greater mid-
490 day transpiration steam). With such a working example in West Africa, the study not only
491 underscores the importance of incorporating the positive effect of aridity on photosynthesis
492 capacity, as predicted by optimality theory, in carbon modelling but also explains how plants
493 arrange water transportation for higher photosynthesis at drier sites. The study also highlights the
494 pivotal role of A_S/A_L in plants long-term adjustment to water shortage.

495 Data availability

496 Figures could be downloaded from

497 https://github.com/Hzhang-ouce/Ghana_rainfall_trait_variation_optimality_github. To reproduce
498 figures, data and R codes mentioned in the main text could also be found in the above repository.

499

500

501 Acknowledgements

502 We thank Nicolas Raab, Natascha Luijken, Ya-Jun Chen, Yu-Heng Sun, Maurizio Mencuccini,
503 Akwasi DGyamfi, Guillaume Delhaye, Dong Ning, Han Wang, Roberto Salguero-Gómez and
504 Sophie Fauset for valuable discussion and assistance with data processing. Y.M. is supported by
505 the Jackson Foundation. H.Z. received Henfrey Scholarship (from St Catherine's College,
506 Oxford) and Tang Scholarship (by China-Oxford Scholarship Fund). The field data collection
507 was funded by a grant award (ERC GEM-TRAIT, grant no. ERC-2012-ADG_20120216) to

Y.M., with additional support for the fieldwork from a Royal Society-Leverhulme Africa Capacity Building Award and Marie Curie Fellowship to I.O. (FP7-2012-IEF-327990-TipTropTrans).

Conflict of interest

The authors have no conflicts of interest to declare that are relevant to the content of this article.

Author contributions

IO, YM, ICP, and HZ designed the research and interpreted the results. DS did the hydraulic modelling. YM, AG, TP, MB, KZ, SAB, JAG, IO, HZ contributed to data collection. HZ carried out the analyses and wrote the paper with inputs and revisions from all co-authors.

Table 1 Traits name, unit, hypotheses and findings from field measurements along the rainfall gradient, Green color denotes consistency between theory and our field data. Orange color denotes inconsistency.

#	Hypotheses	Data	Consistent
	Variables associated with photosynthesis and respiration (Optimality theory)		
1	Toward drier sites, the ratio between leaf-internal and ambient CO2 (ci/ca, %) (from 13C) **decreases**.	Decrease	✓
2	Toward drier sites, Rubisco carboxylation capacity at 25 C° (Vc_{max25}, umol CO2 m2 s-1) **increases**.	Slight increase	✓
3	Toward drier sites, electron transport capacity at 25 C° (J_{max25}, umol CO2 m2 s-1) **increases**.	Slight increase	✓
4	Toward drier sites, light saturated assimilation rate at 400 ppm (Asat, umol CO2 m2 s-1) **increases**.	Increases	✓
5	Toward drier sites, light saturated assimilation rate at 2000 ppm (Amax, umol CO2 m2 s-1) **increases.**	Increase	✓
6	Toward drier sites, leaf dark respiration (Rd, umol CO2 m2 s-1) **increases**.	Increase	✓

7	Toward drier sites, specific stem respiration (Rs, umol CO2 m2 s-1) **increases.**	Increase	✓
	Variables associated with water transportation		
8	Toward drier sites, Sapwood to leaf area ratio (Huber value) (A_S/A_L, cm2 m-2) **increases.**	Increase	✓
9	Toward drier sites, turgor loss point (TLP, MPa) becomes more negative.	More negative	✓
10	Toward drier sites, plant stature, calculated as maximum tree height of a species (H_{max}, m) **decreases**.	Slight decrease	✓
11	Toward drier sites, wood density (g cm-3) and twig density (g cm-3) **increase** (if following the safety-efficiency trade-off).	Slight increase	✓
12	Toward drier sites, potential specific hydraulic conductivity (Kp, kg m-1 Mpa-1 s-1) **decreases** (if following the safety-efficiency trade-off).	Slight increase	
13	Toward drier sites, vessel diameter (μm) **decreases.** (if following the safety-efficiency trade-off).	No trend	
14	Toward drier sites, vessel density (mm-2) **increase.** (if following the safety-efficiency trade-off).	Slight Increase	✓
15	AS/AL and Kp are negatively correlated. (if following safety-efficiency trade-off, and global scale analysis – see introduction)	Positive correlation	
16	For species with high A_S/A_L and Kp, there is high Vcmax (or high Asat)	See Figure 3	✓

'Data' column summarizes patterns in Figure 1. A trend of trait is qualitatively recognized if KOG (dry region) is significantly different to ANK (wet region) while BOB ranks between. 'Slight increase' suggests that the pattern fits the above criteria broadly albeit one plot behaves inconsistently. Colours indicate results that are consistent (green), weakly consistent (light green) and inconsistent (orange) with theoretical expectations. Ticks in the column 'consistent' indicate consistency between hypotheses and data

522

523

524

Study plots properties

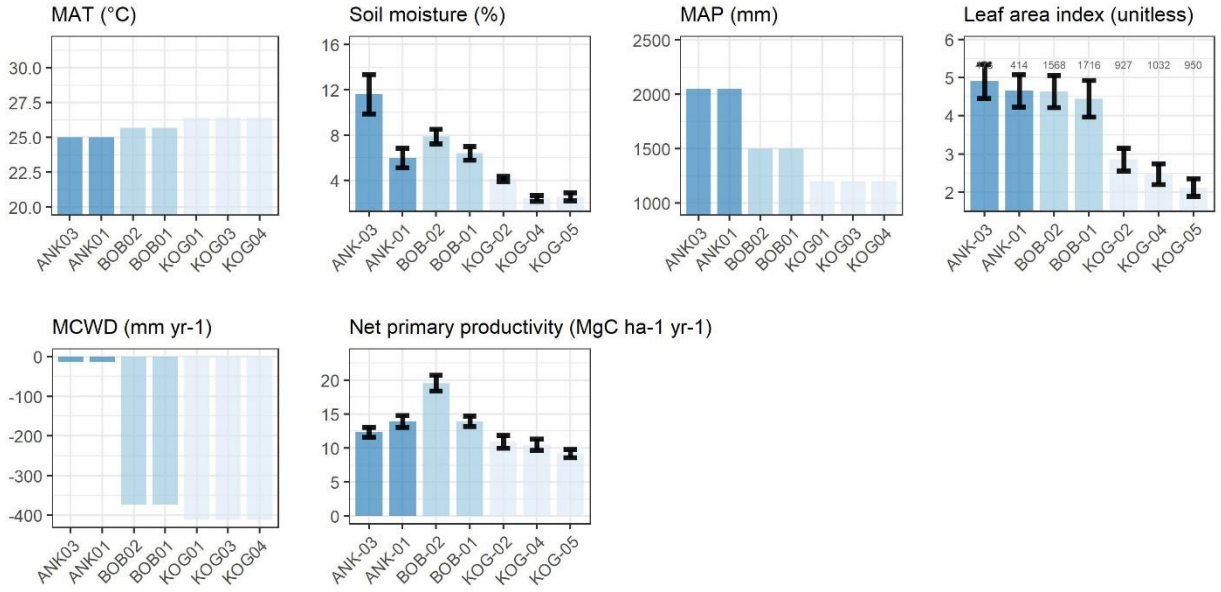

525

Variables associated with photosynthesis and respiration

526

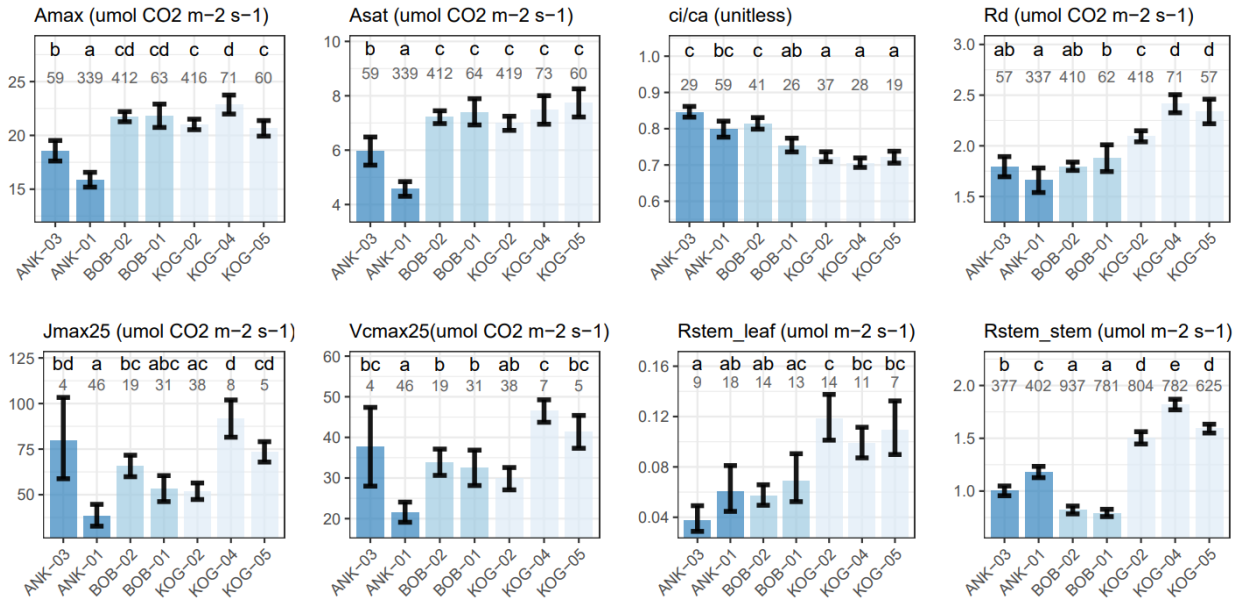

527

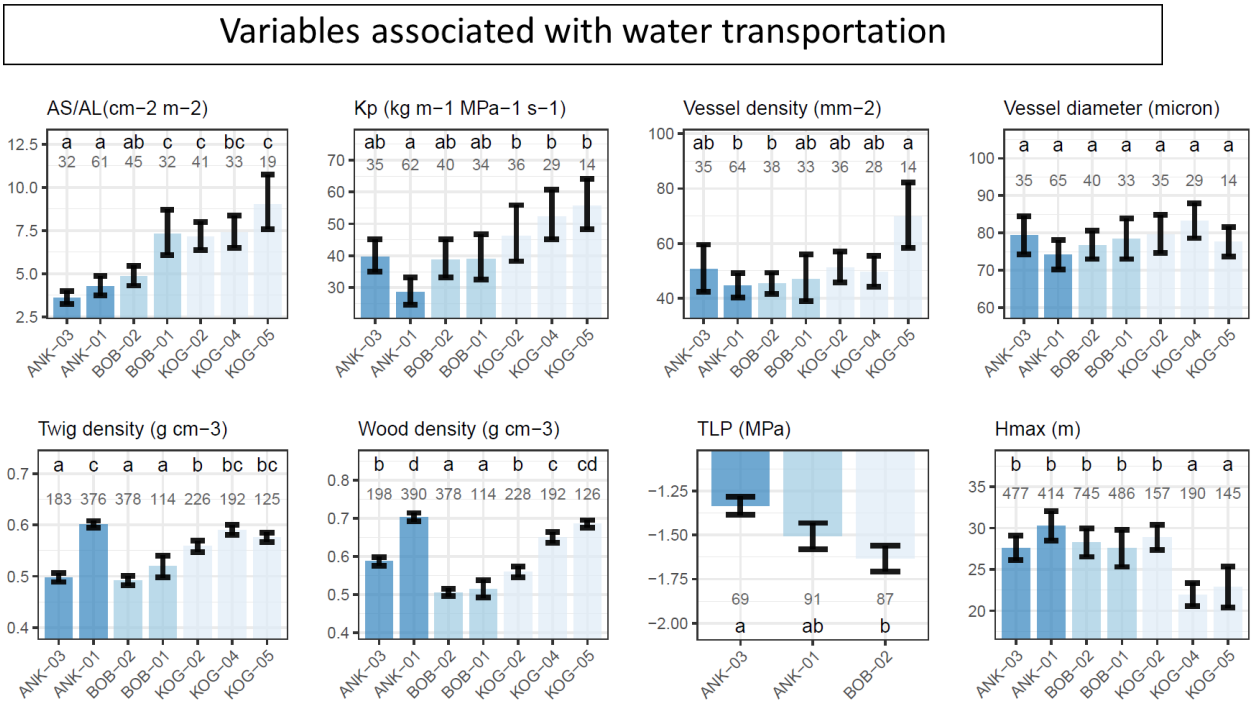

Figure 1 Plot scale community weighted mean (with standard error) from the wettest (left) to the driest (right) plot. Here we show Maximum Cumulative Water Deficit (MCWD), Mean annual air temperature (MAT), mean annual precipitation (MAP) and soil volumetric water content at 12 cm depth (Soil moisture), leaf area index (LAI) and Net primary productivity (NPP) all as annual mean. See Table 1 for the list of plant traits. Forest plots are arrayed from left to right in order of increasing aridity according to MCWD and volumetric water content. The number denotes the number of samples, which could be a leaf, a branch, a tree or a species depending on the variable. The letters denote significance (P<0.05) in plot-to-plot difference.

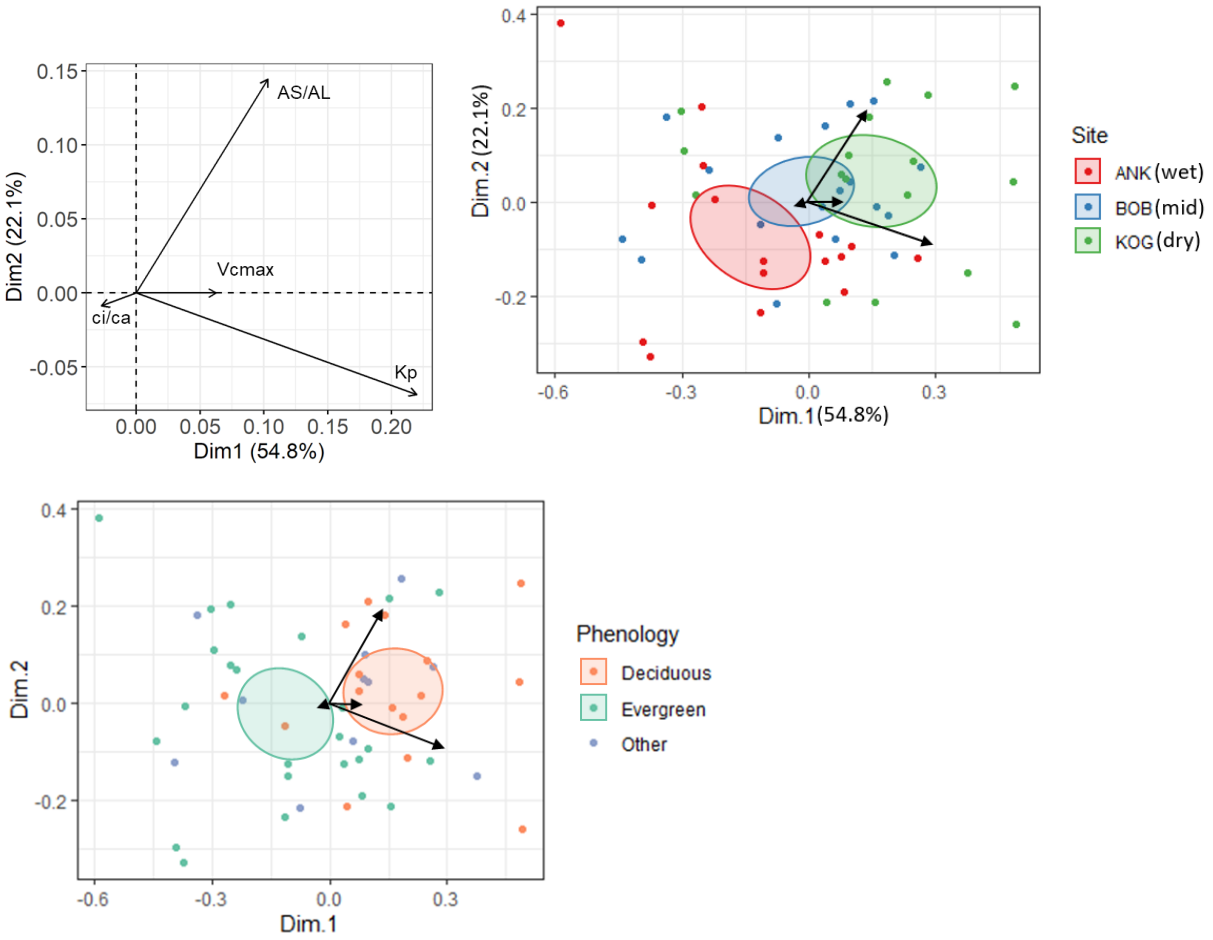

Figure 2 Principal components analysis for Huber value (AS/AL), the ratio between leaf internal and ambient CO2 (ci/ca), Rubisco carboxylation capacity at 25 degree (Vcmax25) and potential specific conductivity (Kp) on species scale. Values are transformed to achieve normal distribution but not standardized to equal variance; therefore the length of arrows denotes the variance of the specific trait. The ellipses for each site are confidence ellipses around group mean points. The PCA axes in all figures are identical. Note that the three figures display the same PCA, but with a different classification of scatter points.

Appendix 1 Field sampling protocol

Please note that the number of samples could be found in Table S 1, Figure 1 and Figure S 3 and thus not repeated here.

The ratio between leaf-internal and ambient CO2, ci/ca (unitless) was estimated from leaf δ13C measurements (the stable isotope ratio relative to a standard material). We first estimated Δ13C the difference between the leaf stable isotope ratio and the atmospheric stable isotope ratio, from δ13C at that place and time according to (Cornwell *et al.*, 2016). Then we estimated ci/ca from Δ13C by equation 11 in (Peng *et al.*, 2020).

Climate and soil variables presented in Figure 1 and Table S1 are field measurements, most of which were sourced from (Moore *et al.*, 2018; Oliveras *et al.*, 2020). Climate variables were recorded by local meteorological station from 2011 to 2015. Soil properties are average across 0-30cm, field measured in 2013 and 2014. Soil volumetric water content (vwc) (%) was measured in the field every month in 2016, using a soil moisture sensor probe over the depth in the forest over the depth 0–12 cm. Soil hydraulic data in Table S2 are model outputs (See Method).

For light saturated assimilation rate at 400 ppm, Asat (umol CO_2 m-2 s-1) and at 2000ppm, Amax (umol CO_2 m-2 s-1), The branch that had been cut was promptly placed in water and recut. To measure leaf gas exchange traits, an open flow gas exchange system (LI-6400XT, Li-Cor Inc., Lincoln, NE, USA) was used. Three leaves were selected from each tree and analyzed for Asat and Amax, as well as dark respiration (R_d) (μmol m–2 s–1 for all photosynthesis traits). The photosynthetic photon flux density was set at 2000 μmol m-2 s-1, with the exception of dark respiration measurements (0 μmol m-2 s-1). The block temperature was kept constant at 30º C throughout the sampling period, which was similar to the ambient air temperature. More information could be found from supporting information in (Aguirre-Gutiérrez *et al.*, 2019; Oliveras *et al.*, 2020). The above traits were sampled each month from October 2014 to September 2016.

To determine leaf mass per area, LMA (m-2 kg-1), nitrogen content by area, N_{area} (g m-2), nitrogen content by mass, N_{mass} (g/kg), phosphorus content by area, P_{area} (g m-2), and phosphorus

content by mass, P_{mass} (g/kg), we selected three fully-grown trees that emerged from the canopy (total of 298 trees) for each species in a given site. Within each tree, we randomly chose three mature leaves from a fully sunlit branch that were not in the process of senescing. The leaves were then dried in an oven at 70°C until a constant mass was reached. Total leaf lamina area (cm2) was calculated by scanning images using NIH ImageJ (http://rsbweb.nih.gov/ij/) and a custom MATLAB script (https://github.com/bblonder/leafarea). LMA was calculated by dividing the dried leaf mass by the leaf area. Part of these data were reported in (Gvozdevaite, 2018; Oliveras *et al.*, 2020). Data reported in this study are slightly different to the above two studies because there is more sampling in this study. Samples were taken each month from October 2014 to September 2016.

To measure maximum rate of electron transport at 25 ºC J_{max25} (umol CO2 m-2 s-1) and maximum rate of carboxylation at 25 ºC V_{cmax25} (umol CO2 m-2 s-1), we sampled one individual tree per species within each study plot to generate A-Ci curves, which show the photosynthetic response to changes in substomatal CO2 concentration (Ci). CO2 concentration was changed in the following sequence: 400, 300, 200, 100, 50, 400, 600, 800, 1200, 1500, and 2000 µmol m-2 s -1. The photosynthetic photon flux density was set at 2000 µmol m-2 s-1, and the block temperature was kept constant and closest to ambient throughout the sampling period at 30ºC. We used the A-Ci curve fitting method and followed the procedure described in detail in Appendix B of Domingues et al. (2010) which extracts V_{cmax} and J_{max} values. To enable comparison of our data and findings with the wider literature on photosynthetic capacity variability, we scaled the measured and estimated values of V_{cmax} and J_{max} to a reference temperature of 25°C following Sharkey et al. (2007). We further refer to the scaled values as V_{cmax25} and J_{max25} in the text. V_{cmax25} and J_{max25} are collected in October 2015. The field campaign did not finish at site ANK-03 leading to very little number of samples at this site.

To calculate sapwood area to leaf area, or Huber value, AS/AL (cm-2 m-2), we first determine leaf area (AL) of a sampled terminal, sun-exposed shoots from the outer canopy. We scanned the adaxial side of the leaf lamina (without petiole) on a Canon Lided220® flatbed scanner and analysed the images using a Matlab code that can be found at https://github.com/bblonder/leafarea Neyret et al. (2016). The total leaf area per branch (AS/AL)

606 was determined with the assumption that the branch diameter (without bark) corresponded to
607 sapwood area. Samples are collected in October 2015.

608 For structural traits, including twig density (g cm-3), vessel density (mm-2), average vessel
609 diameter (μm) and potential specific hydraulic conductivity, Kp (kg m-1 MPa-1 s-1), we sampled
610 ~8-10mm diameter twigs, on three replicates per species (Gvozdevaite, 2018). Cross sections
611 about 20-50μm were made using a sliding microtome, stained in safranin O and alcian blue, and
612 permanently mounted on a microscopic slide. A pie shaped segment stretching from pith to
613 cambium was photographed using OptronicsMicrofire camera mounted on Olympus BX-50
614 microscope and PictureFrame software. All vessels within a pie region were marked and
615 coloured using magic wand tool (GIMP, http://gimp.org) and interactive pen display (Wacom
616 Cintiq 22HD). Vessel area, average diameter (average of minimum and maximum diameters)
617 and pie region area were measured using ImageJ. Next, average diameters of all vessels per
618 given pie area were averaged resulting in sample average vessel diameter (VD) which was then
619 used in the analyses. Vessel density (ρV) was calculated by dividing the total number of vessels
620 in an analyzed pie section by the area of that pie section. Lastly, we calculated Kp using the
621 Hagen-Poiseuille equation as per Poorter et al. (2010). Twigs were dried for at least 72 hours at
622 105°C and mass was measured on a precision balance. The twig density was calculated as dry
623 mass divided by the volume of soaked wood. Samples are collected in October 2015.

624 For maximum tree height of a species, Hmax (m), in January 2020, we measured the tree height
625 of each tree using a digital clinometer in the forest plot (with diameter at breast height larger than
626 10cm).

627 For turgor loss point, TLP (MPa), a sunlit branch with fully grown leaves was collected and re-
628 cut while submerged in water. The branch was then rehydrated overnight, covered with a black
629 plastic bag sprinkled with water on the inside, and left to rehydrate for approximately 15 hours.
630 To generate pressure-volumn curves, paired measurements of leaf water potential and leaf mass
631 were repeatedly taken after intervals of bench drying, resulting in 9 to 12 points per curve. The
632 leaves were scanned to obtain their area and then oven-dried at 60 degrees Celsius for 3 days to
633 obtain their dry mass. PV curves were fitted to extract TLP using codes in (Raab, 2020). TLP
634 was collected in August 2019. Pressure-volume curves are measured in October 2015.

Wood density was provided by Forestplot.net who sourced information from (Zanne *et al.*, 2009). In Appendix 4, we also compared data collected from Ghana with AS/AL from (Mencuccini *et al.*, 2019b)and vessel diameter from xylem functional traits database (Choat *et al.*, 2012).

Stem respiration per steam area (Rs_stem) was measured using a closed dynamic chamber method, from 25 trees distributed evenly throughout each plot at 1.3 m height with an IRGA (EGM-4) and soil respiration chamber (SRC-1) connected to a permanent collar. As we know tree height of each tree, Rs_stem could be converted to stem respiration per leaf area (Rs_leaf) using tree height and AS/AL. Assuming trees have a cylindrical shape, we have Rs_leaf= Rs_stem *4 * AS/AL * H / DBH, where AS/AL is Huber value, H is tree height and DBH is diameter at breast height. We calculated Rs_leaf because most of the traits and theories involved in this study were expressed on per leaf area basis. Stem respiration was measured every three months from 2014 to 2016.

Leaf area index (LAI) was estimated from hemispherical images taken with a Nikon 5100 camera and Nikon Fisheye Converter FC-E8 0.21x JAPAN near the center of each of the 25 subplots in each plot in each site, at a standard height of 1 m, and during overcast conditions. 22,000 photos were collected in total, every month during 2016-2017(ANK), 2012-2017 (BOB&KOG). Photos were processed using machine learning-based software 'ilastik' (Berg *et al.*, 2019) for pixel classification and CANEYE (Demarez *et al.*, 2008) for leaf area index calculations. The exposure procedure followed (Zhang *et al.*, 2005) and GEM manual (Malhi *et al.*, 2021) (http://gem.tropicalforests.ox.ac.uk). The following parameters were supplied to CANEYE.

(1) P1 = angle of view of the fish eye divided by the amount of pixels from centroid of the fish eye circle to where horizon is on the image.
(2) angle of view = 90 degree, in which case, the edge of the photo is the horizon and the centroid of the image is zenith.
(3) COI = 80, consideration of field is 80 degrees, we don't want the edge of the photo because it is not clear and sometimes obscure by tall grasses or saplings.
(4) Sub sample factor =1
(5) Fcover = 20 degree, this is to calculate the percentage of black pixels within central 20-degree ring. We used this to understand the relative openness of canopy for the given image. It is not relevant to LAI

(6) PAIsat = 10, When a pixel is completely black, mathematically, the leaf area index (LAI) is infinite. As we provide CANEYE 25 subplot images for each estimation of LAI, this means all 25 subplot images show black at a given pixel. To address this 'infinite'issue, we use a value of 10 for LAI in such cases. This value is based on the guess that, the densest point in a tropical forest should have an LAI of 10.

(7) Latitude 0 and Day of year a random number (not relevant for tropical site LAI)

Then, we extract output from CANEYE using software R. We chose the latest method of LAI calculation offered by CANEYE, 'CE V6.1 True PAI'. CANEYE reported one LAI value per method (4 methods) per plot per site per month, as a synthesis across 25 subplots images. As systematic error is dominating in LAI calculation, we take the standard deviation of LAI across four methods as the uncertainty for LAI.

Appendix 2 Study Sites, the aridity gradient

679

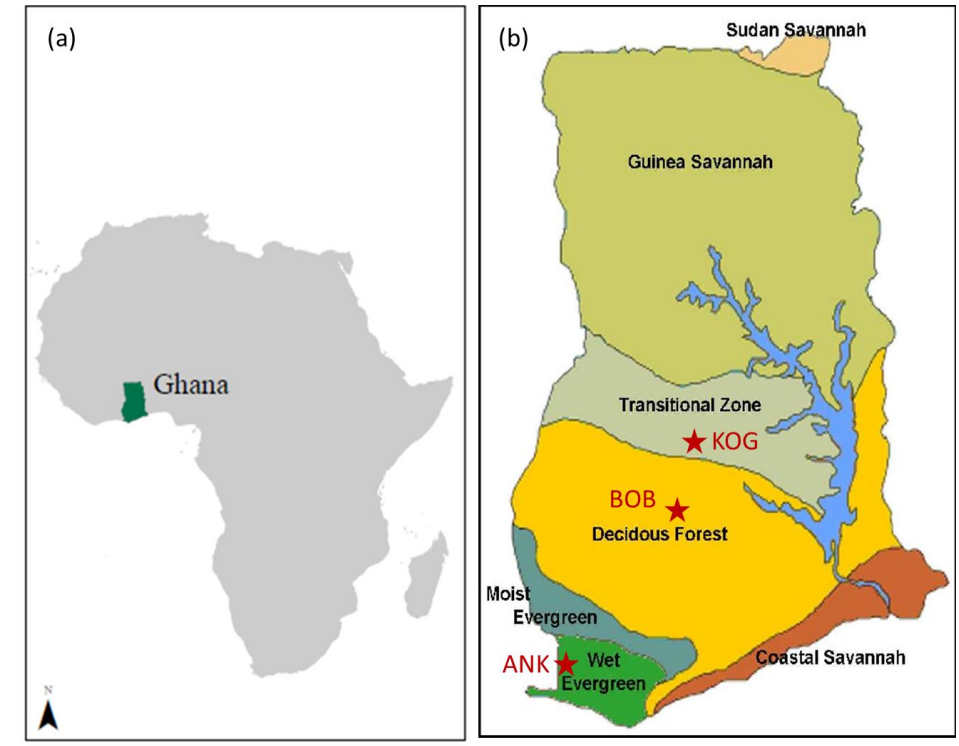

680

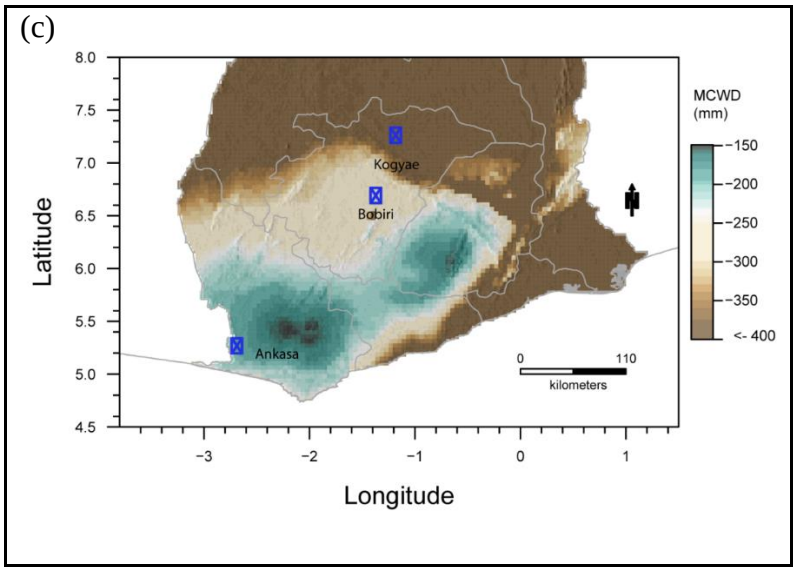

681 *Figure S 1Map of the location of (a) Ghana within the African continent (b) and the study sites*

682 *and forest types in Ghana (Appiah* et al.*, 2014). (c) showed study sites over a map of maximum*

683 *climate water deficit (MCWD) (Aguirre-Gutiérrez* et al.*, 2019).*

684

Figure S 2 Photo of KOG02 (dry site), KOG05(dry site), ANK03 (wet site), and BOB01 (mid site). All photos were taken in January 2022 by Huanyuan Zhang-Zheng

Table S 1Summary information of plot characteristics

		Wet >>>>>>>>>>>>>>>>>>>>>>>>>>>>>>>>>>>> Dry						
Plot		ANK-01	ANK03	BOB-01	BOB-02	KOG02	KOG-04	KOG05
Lat		5.27	5.27	6.7	6.69	7.26	7.3	7.3
Long		-2.69	-2.69	-1.32	-1.34	-1.15	-1.18	-1.16
Elev	(m)	114	86	277	281	229	230	221
PPFD	(mol /m2/day)	30.97	30.97	35.58	35.58	44.26	44.26	44.26
MAP	(mm)	2050	2050	1500	1500	1200	1200	1200
MAT	(°C)	25	25	25.7	25.7	26.4	26.4	26.4
MCWD	(mm/yr)	-13	-13	-374	-374	-412	-412	-412
Vegetation type		LR	SLR	SemR	SemR	SSF	STF	WS
BA	(m2/ha)	28	25.8	22.9	31.1	17.5	13.5	12.4
Ind	(#/ha)	59	31	27	41	36	33	22
Trees	(#/ha)	477	414	745	486	157	190	145
Sp/Gen/Fam		35/29/22	13/13/9	16/13/8	14/13/8	15/14/10	11/11/7	7/6/5
P	(mg/kg)	146.8	109.7	77.8	258.3	67.2	74.6	81.9
N	(%)	0.17	0.12	0.09	0.16	0.06	0.05	0.04
C	(%)	2.61	1.91	0.8	1.71	0.72	0.67	0.62
Ca	(mg/kg)	26.8	40	306.3	657.6	378.9	308	237.1
K	(mg/kg)	32.3	33.7	47.6	49	42.5	35.6	28.7
Mg	(mg/kg)	42	29.2	79.7	133.7	75.6	78.7	81.3
Sand	(%)	63.1	75.9	64.2	46.7	82.4	79.7	76.9
Clay	(%)	21.6	12.8	6.7	28.8	2.3	3.3	4.3

Plot coordinates (Latitude[Lat]/Longitude[Long]) are provided in degrees. Elev, elevation; MAP, mean annual precipitation; PPFD, photosynthetic photon flux density, calculated from shortwave radiation *0.5; MAT, mean annual temperature; MCWD, Maximum Cumulative Water Deficit; Vegetation type (LR, lowland rainforest; SLR, semi-flooded lowland rainforest; SemR, semi-deciduous rainforest; SSF, seasonal semi-deciduous forest; STF, seasonal transitional rainforest; WS, woodland savanna); BA, total basal area in a plot; Ind, number of tree individuals sampled; Trees, total number of trees larger than 10cm diameter at breast height; Soil nutrients (P, phosphorus; N, nitrogen; C, carbon; Ca, calcium; Mg, magnesium), and soil percentage of sand (Sand) and of clay (Clay). Data from (Moore *et al.*, 2018; Oliveras *et al.*, 2020)

Table S 2 Rsplash model outputs, which simulate hydrology from climate, typography and soil property. vwc_mean and vwc_sd are mean and standard deviation of soil volumetric water content (unitless fraction); Se_mean and Se_sd are the mean and standard deviation of relative soil moisture saturation (Θ) (unitless fraction); Alpha_mean and Alpha_sd are mean and standard deviation of vegetation water stress index (α) (unitless fraction, calculated as AET/PET); Aet is actual evapotranspiration (mm year-1); Pet is potential evapotranspiration (mm year-1); ro is runoff (mm year-1); cond is condensation (mm year-1); MAP is mean annual precipitation (mm year-1), MAT is mean annual air temperature (degree Celsius), VPD is vapor pressure deficit (kpa, annual stats); SAT: volumetric water content at saturation m3 m-3; perc: percolation or deep drainage, or vertical drainage (mm/year); FC is volumetric water content at 33kPa (field capacity) m^3/m^3; WP, volumetric water content at 1500kPa (permanent wilting point) m^3/m^3; AWC: plant available volumetric water content (FC-WP); Ksat, Saturated hydraulic conductivity (mm/hr)

Plot	ANK-01	ANK-03	BOB-01	BOB-02	KOG-02	KOG-04	KOG-05
Site	Ankasa	Ankasa	Bobiri	Bobiri	Kogyae	Kogyae	Kogyae
vwc_mean	0.173647	0.309652	0.288372	0.417	0.174785	0.152259	0.134706
vwc_sd	0.017241	0.085336	0.032128	0.045303	0.029734	0.02364	0.018203
Se_mean	0.379521	0.581384	0.580031	0.786519	0.3387	0.301315	0.272344
Se_sd	0.037682	0.160223	0.064623	0.085447	0.057618	0.046783	0.036803
alpha_mean	0.630998	0.583154	0.655883	0.70185	0.401261	0.366604	0.338958
alpha_sd	0.024953	0.038648	0.02599	0.005342	0.013719	0.010825	0.00929
aet	863.1792	805.3301	951.0688	1016.294	658.4057	606.0918	559.005
pet	1366.693	1378.178	1448.611	1447.996	1641.281	1654.57	1651.407
ro	0	177.2069	0	70.2051	0	0	0
cond	35.00537	32.64697	34.66683	34.9216	47.13504	44.43666	45.14205
perc	48.78369	140.6087	12.80651	156.903	272.1005	192.8297	71.75027
MAP_mean	2183.329	2183.329	1297.797	1297.797	1327.496	1327.496	1327.496
MAP_sd	548.3388	548.3388	96.80984	96.80984	91.86095	91.86095	91.86095
MAT_mean	25.02057	25.02057	26.04887	26.04887	26.75565	26.75565	26.75565
MAT_sd	0.114074	0.114074	0.320538	0.320538	0.277137	0.277137	0.277137
VPD_mean	0.099453	0.099453	0.465912	0.465912	0.756213	0.756213	0.756213
VPD_sd	0.108151	0.108151	0.290293	0.290293	0.726797	0.726797	0.726797
PET/MAP	0.625968	0.631228	1.116207	1.115734	1.236373	1.246384	1.244001
SAT	0.293072	0.517389	0.453959	0.484107	0.515887	0.505159	0.494013

FC	0.130408	0.252317	0.216695	0.276332	0.198493	0.194701	0.190016
WP	0.061419	0.103204	0.096532	0.141651	0.057346	0.059782	0.061278
AWC	0.107705	0.1535	0.1316	0.1475	0.141191	0.134961	0.128895
Ksat	87.86493	115.5978	96.32671	60.17225	205.6295	188.7933	174.9063

Appendix 3 Information associated with leaf economy

Leaf economy traits have been published (Gvozdevaite *et al.*, 2018; Oliveras *et al.*, 2020). Data reported in this study are slightly different to the above two studys because there are more sampling in this study. Samples were taken each month from October 2014 to September 2016. Data here are provided for completeness and for future researchers 'convenience.

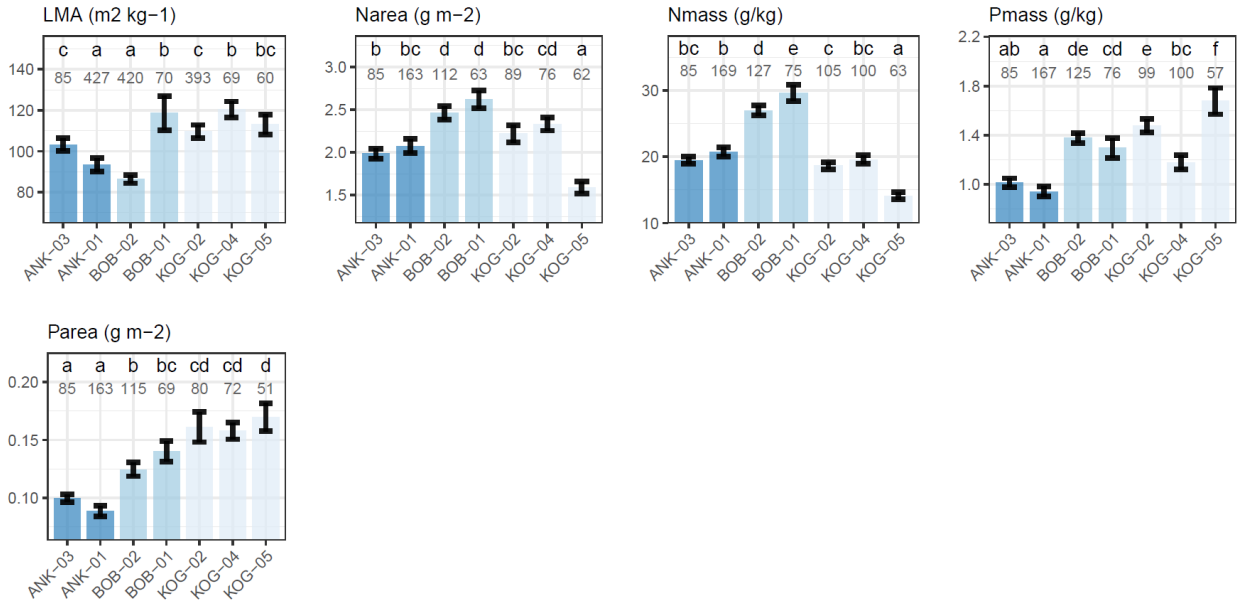

Figure S 3 Community weighted mean (with standard error) of variables associated with leaf economy from wet to dry plots. Plots were ordered from left to right according to the

description in the first paragraph of results. The number denotes the number of samples, which could be a leaf, a branch or a tree etc. The letters denote significance (P<0.05) in plot-to-plot difference. (Oliveras et al.*, 2020)*

Appendix 4 Report on Hypothesis 15

We hypothesized that the product of K_P (specific xylem hydraulic conductivity) and A_S/A_L (sapwood to leaf area) vary less than K_P or A_S/A_L themselves, and there is a trade-off (negative correlation) between K_P and AS/AL. As the trade-off between Ks (well associated with K_P) and A_S/A_L has been observed on a global scale (Mencuccini *et al.*, 2019b), here we also plot K_P versus A_S/A_L for readers' convenience in comparison with measurements from Ghana aridity gradient. We estimated K_P for species reported in (Mencuccini *et al.*, 2019b) by collecting vessel diameter and vessel density from XFT database (Choat *et al.*, 2012), with the same calculation method as K_P of Ghana aridity gradient.

For Ghana, both hypotheses were rejected, as we see a positive correlation between K_P and A_S/A_L (slope = 0.95, R-squared : 0.0598, P-value : 0.0224) and the coefficient of variance is found largest for $K_P * A_S/A_L$.

For a global dataset (Mencuccini et al., 2019), there is a negative correlation between K_P and A_S/A_L (slope =-0.638, R-squared: 0.153, P-value : <0.001) which agreed with the hypothesis but the coefficient of variance of $K_P * A_S/A_L$ is still larger than that of either K_P or A_S/A_L.

Therefore, hypothesis 15 in Table 1 is rejected in this study. The negative correlation between K_P and A_S/A_L emerge on global scale probably because of confounding effect with other environmental variables. The different patterns emerged at different scale could also result from a Simpson's paradox. For example, the drier sites (KOG) have higher K_P , higher twig density and higher wood density than the wetter sites on site scale (Figure 2), but we also found K_P negatively correlated with twig density on species scale (Figure S5)

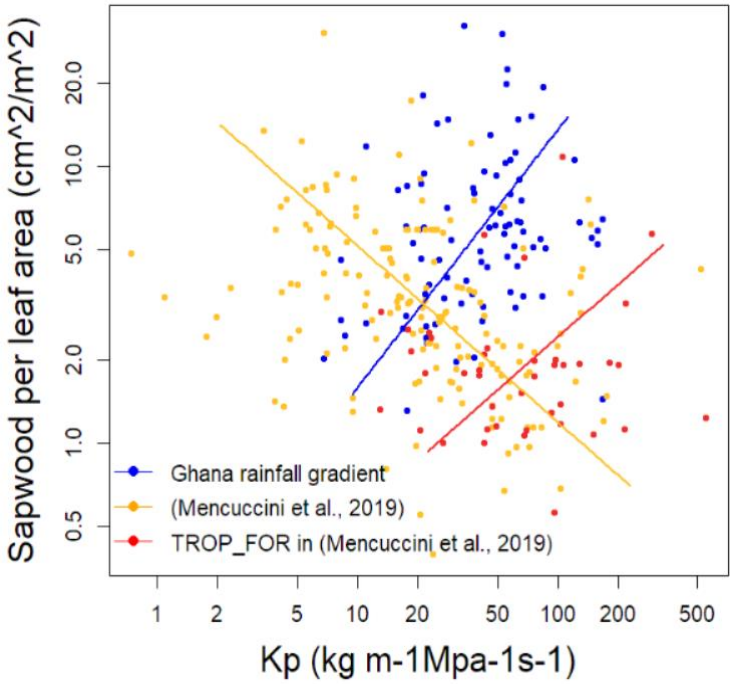

739

740 *Figure S 4 The correlation between sapwood to leaf area (AS/AL) and potential sapwood*
741 *hydraulic conductivity (Kp) for Ghana aridity gradient (ANK, BOB and KOG all together) and*
742 *species included in (Mencuccini* et al*., 2019b). The figure was drawn on species scale (one*
743 *scatter point is one species).*

744

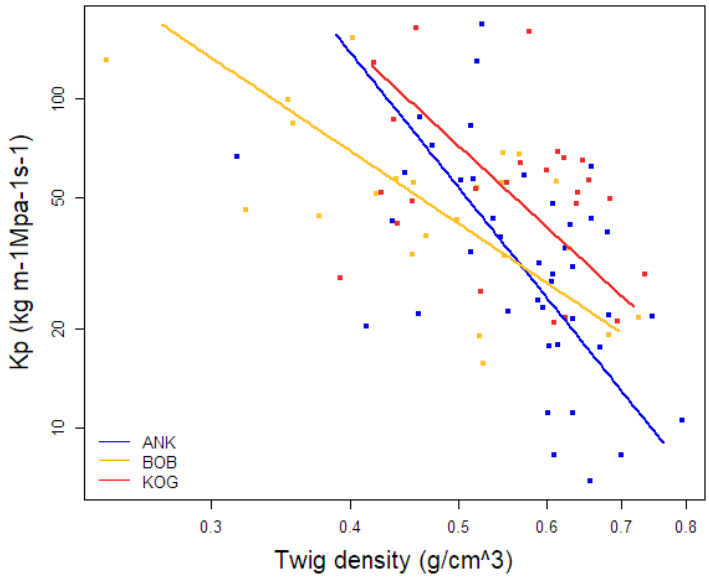

745

746 *Figure S 5 The correlation between twig density (g/cm3) and potential sapwood hydraulic*
747 *conductivity (Kp) for site ANK, BOB and KOG. The figure was drawn on species scale (one scatter*
748 *point is one species).*

749

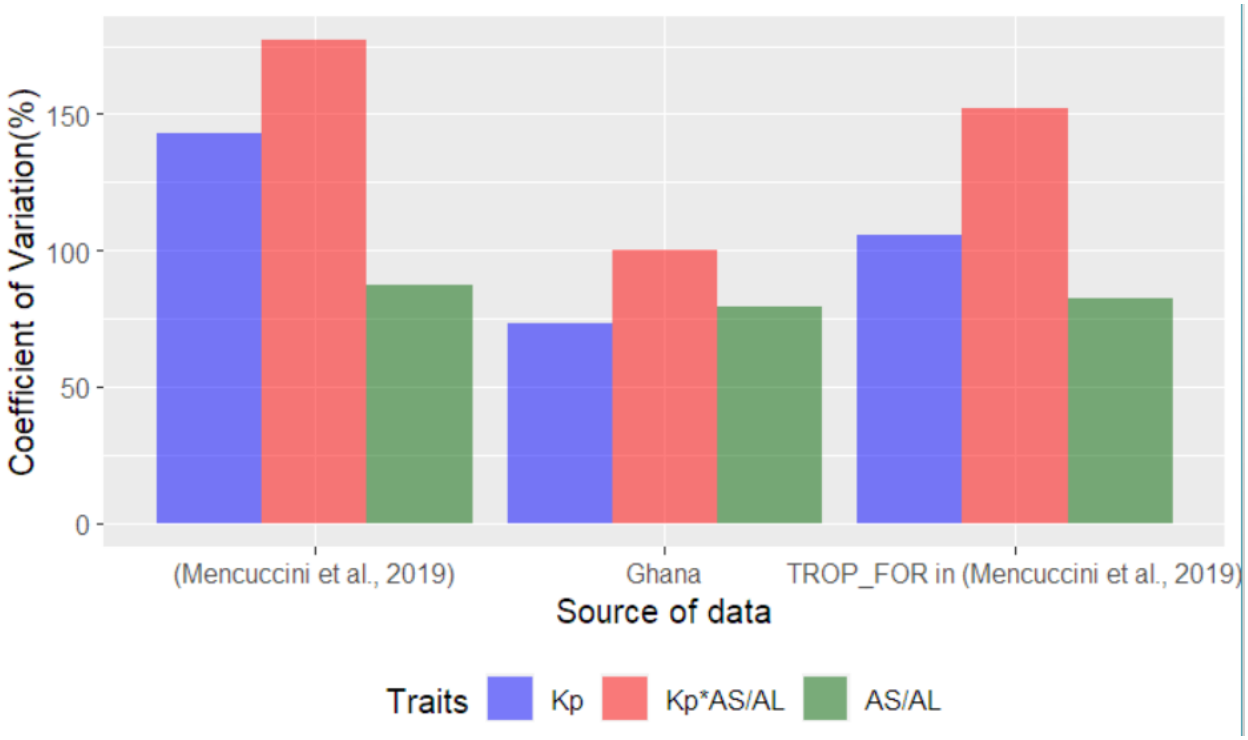

Figure S 6 Coefficient of variation (%) for data points shown in figure S6, potential sapwood hydraulic conductivity (Kp), sapwood area to leaf area (AS/AL) and the product of Kp and AS/AL

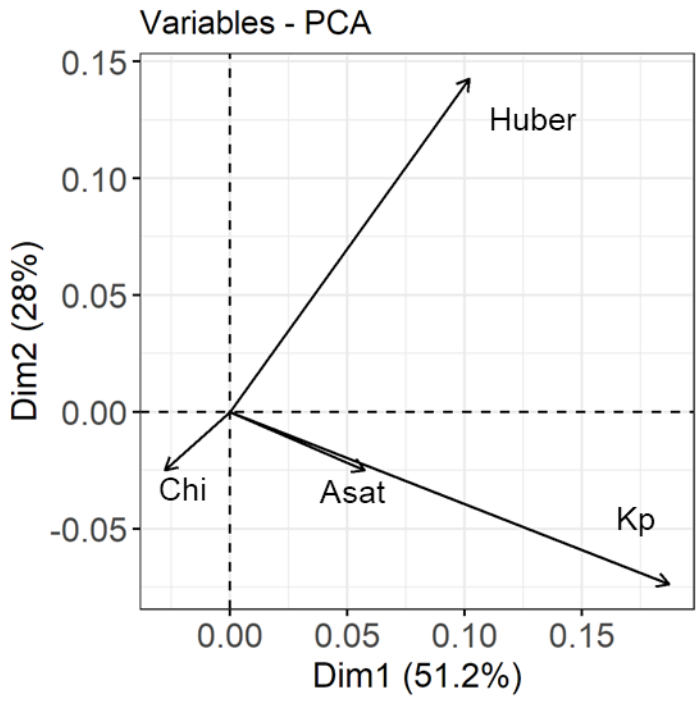

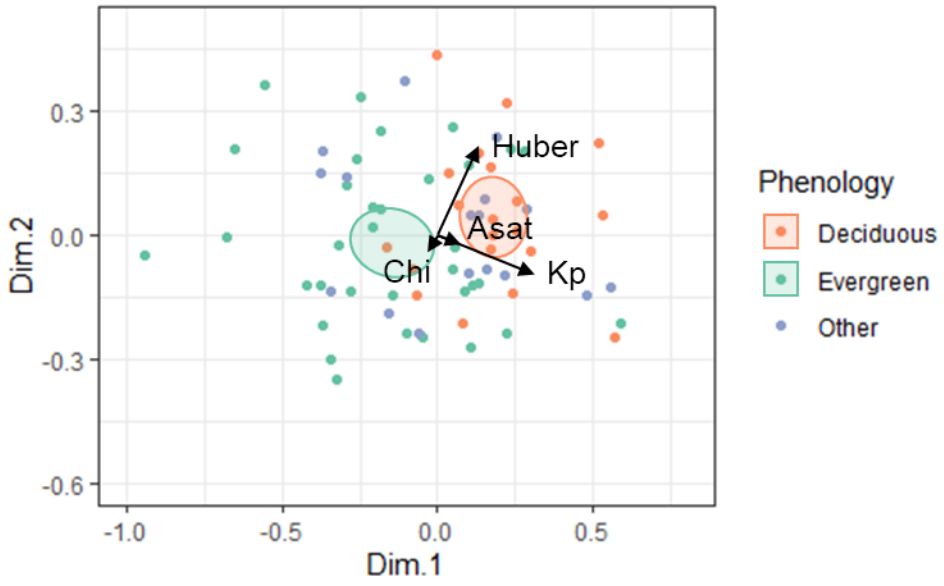

754

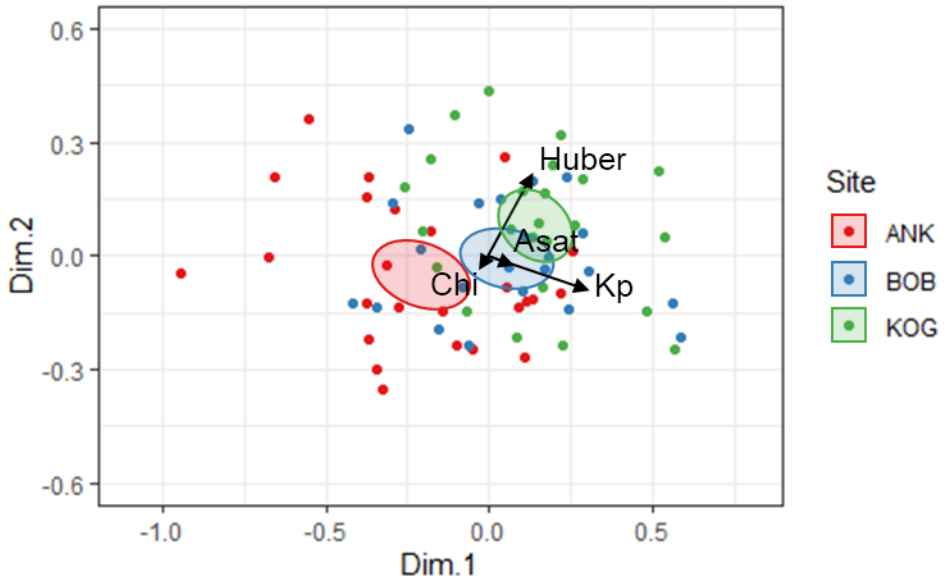

Figure S 7 Principal components analysis for A_S/A_L , ci/ca, Asat and Kp. Pleaser also see Figure 2

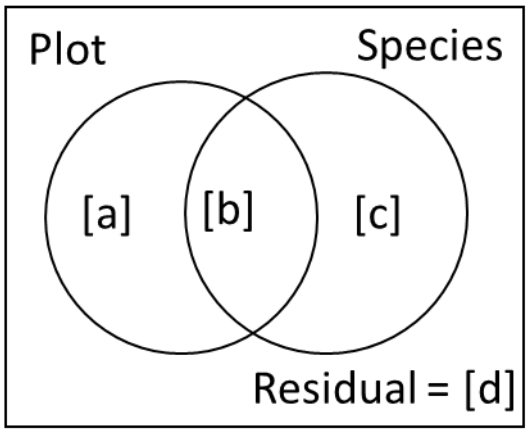

[a] Variance incurred by changing plot for the same species

[b] Variance incurred by changing plot and changing species

[c] Variance incurred by changing Species but not plot (inter-specific variance in a plot)

[d] Variance incurred by anything else but not changing plot and not changing species. It includes intra-specific variation (e.g., changing measurement leaves) and measurement error because for most of the traits, [d] exist only when multiple measurements were collected for one species. If the changing species induced variance [c] is larger than [d], it is safe to conclude that the variation of trait (overall in Ghana) is dominated by changing species, instead of intra-specific variation

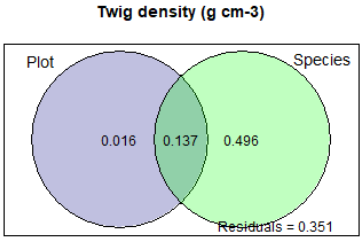

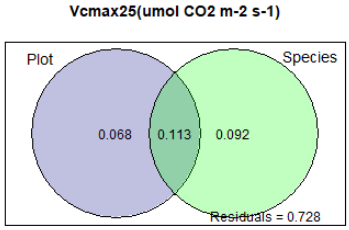

766

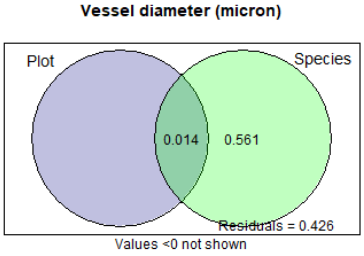

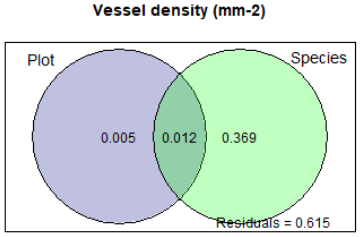

767

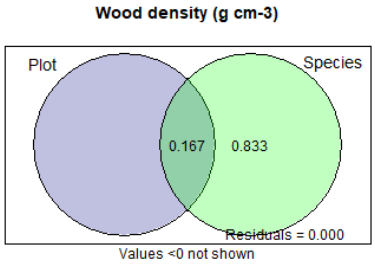

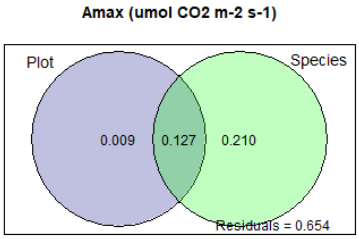

768

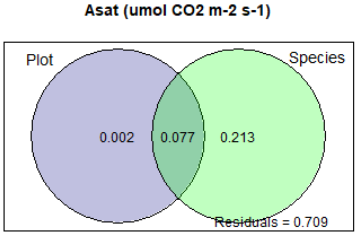

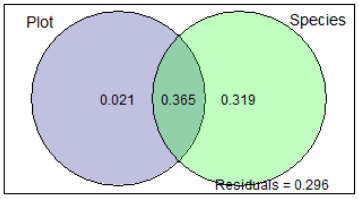

769

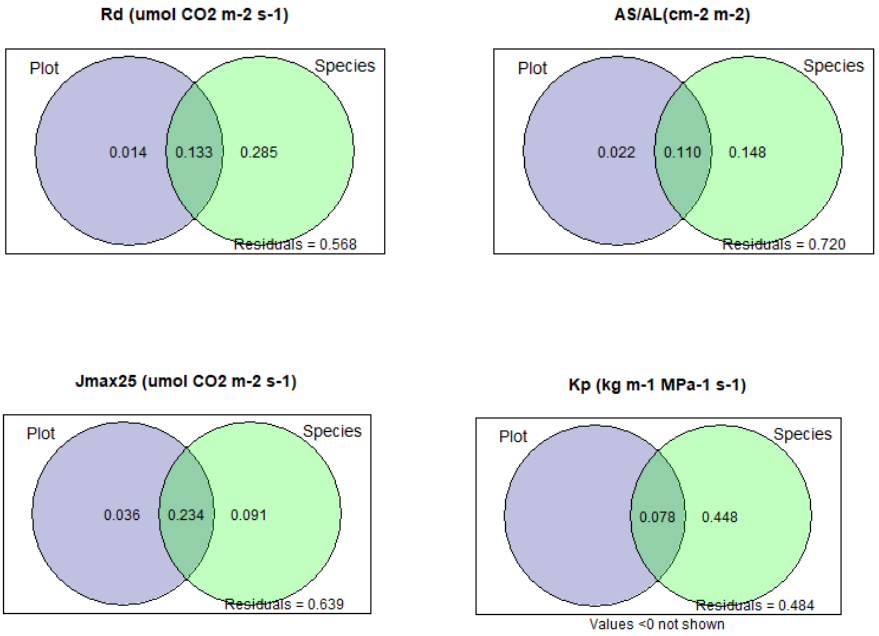

Figure S 8 Variance partitioning into plot and species. Please see table 1 for definition of traits. Meanings of each number in the circles are explained in the top panel. Note that Vcmax, LMA

Narea and Parea from the same plots were published in (Gvozdevaite et al.*, 2018), and Asat Amax LMA, Nmass and Pmass from the same plots were published in (Oliveras et al., 2020). Values are not mathematically identical due to (1) different methods of variance partitioning and (2) one more year sampling than the previous publications*

Appendix 5 Other figures

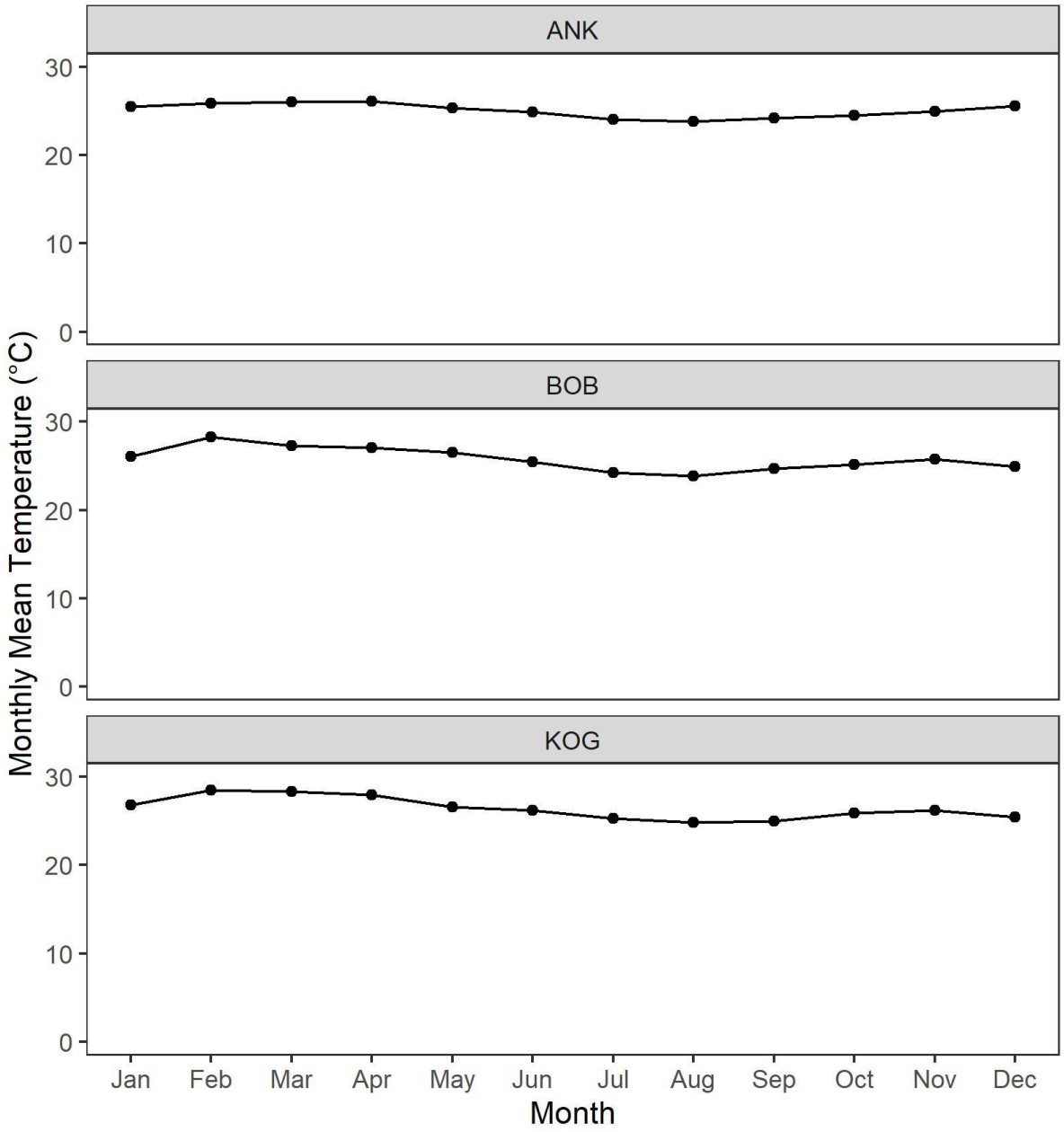

784

785 *Figure S 9 Monthly mean temperature at study sites ANK (wet site), BOB (mid site) and KOG (dry*

786 *site), measured by in-situ climatological stations.*

787

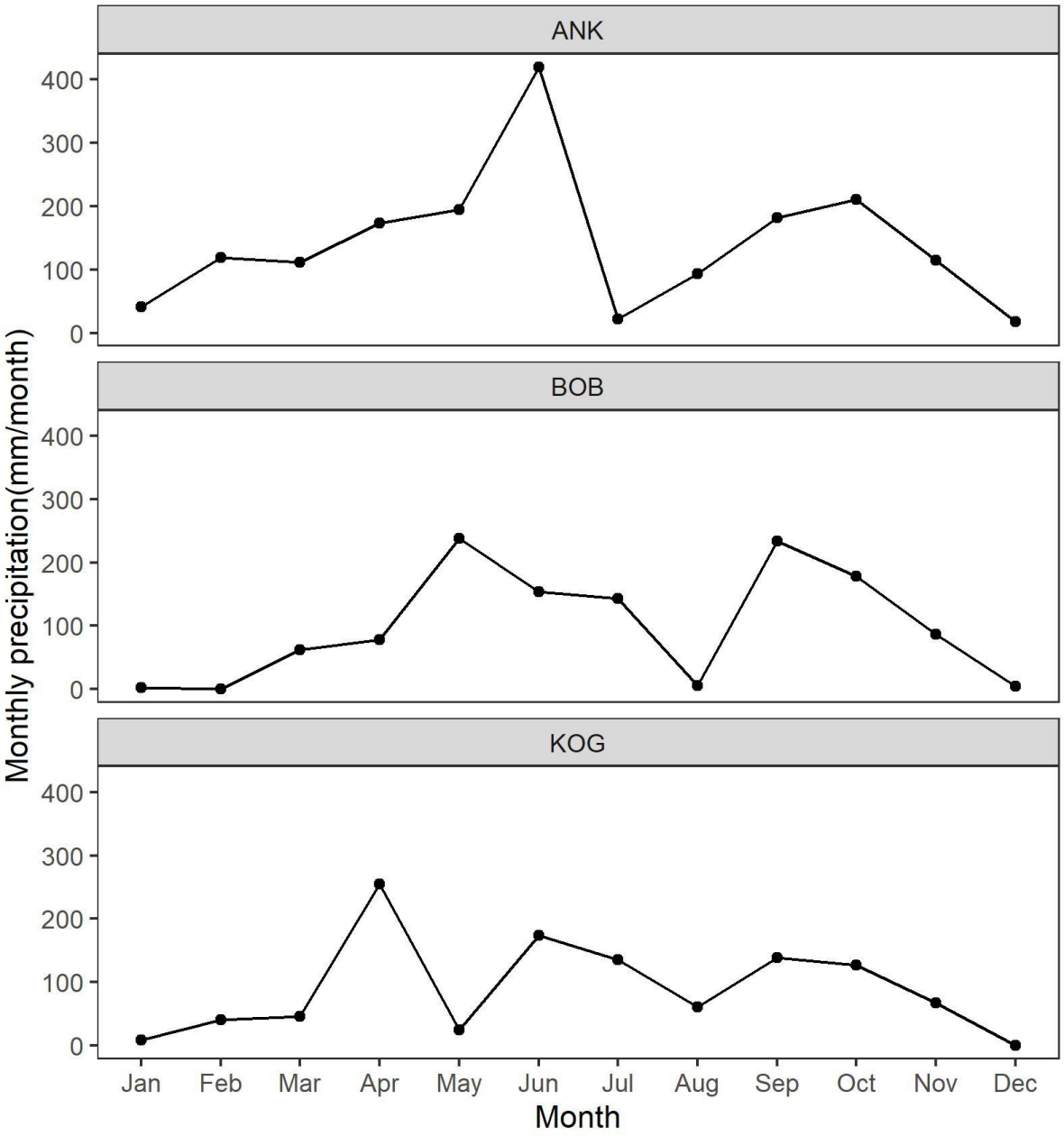

788

789 *Figure S 10 Monthly precipitation (mm/month) at study sites ANK (wet site, measured in 2011),*

790 *BOB (mid site, measured in 2013) and KOG (dry site, measured in 2014), measured by in-situ*

791 *climatological stations.*

792

793

794 ## References

795

796 **Aguirre-Gutiérrez J, Oliveras I, Rifai S, Fauset S, Adu-Bredu S, Affum-Baffoe K, Baker**
797 **TR, Feldpausch TR, Gvozdevaite A, Hubau W, *et al.* 2019**. Drier tropical forests are
798 susceptible to functional changes in response to a long-term drought. *Ecology Letters* **22**: 855–
799 865.

800 **Appiah D, Osman B, Boafo J**. **2014**. Land Use and Misuse; Human Appropriation of Land
801 Ecosystems Services in Ghana. *International Journal of Ecosystem* **4**: 24–33.

802 **Atkin OK, Bloomfield KJ, Reich PB, Tjoelker MG, Asner GP, Bonal D, Bönisch G,**
803 **Bradford MG, Cernusak LA, Cosio EG, *et al.* 2015**. Global variability in leaf respiration in
804 relation to climate, plant functional types and leaf traits. *New Phytologist* **206**: 614–636.

805 **Bahar NHA, Ishida FY, Weerasinghe LK, Guerrieri R, O'Sullivan OS, Bloomfield KJ,**
806 **Asner GP, Martin RE, Lloyd J, Malhi Y, *et al.* 2017**. Leaf-level photosynthetic capacity in
807 lowland Amazonian and high-elevation Andean tropical moist forests of Peru. *New Phytologist*
808 **214**: 1002–1018.

809 **Bartlett MK, Scoffoni C, Sack L**. **2012**. The determinants of leaf turgor loss point and
810 prediction of drought tolerance of species and biomes: A global meta-analysis. *Ecology Letters*
811 **15**.

812 **Bauman D, Fortunel C, Delhaye G, Malhi Y, Cernusak LA, Bentley LP, Rifai SW, Aguirre-**
813 **Gutiérrez J, Menor IO, Phillips OL, *et al.* 2022**. Tropical tree mortality has increased with
814 rising atmospheric water stress. *Nature*.

815 **Beerling DJ, Quick WP**. **1995**. A new technique for estimating rates of carboxylation and
816 electron transport in leaves of C3 plants for use in dynamic global vegetation models. *Global*
817 *Change Biology* **1**: 289–294.

Berg S, Kutra D, Kroeger T, Straehle CN, Kausler BX, Haubold C, Schiegg M, Ales J, Beier T, Rudy M, *et al.* 2019. ilastik: interactive machine learning for (bio)image analysis. *Nature Methods* **16**.

Bittencourt PRL, Pereira L, Oliveira RS. **2016**. On xylem hydraulic efficiencies, wood space-use and the safety–efficiency tradeoff. *New Phytologist* **211**: 1152–1155.

Björkman O. **1981**. Responses to Different Quantum Flux Densities. *Physiological Plant Ecology I*: 57–107.

Brodribb TJ, Feild TS. **2000**. Stem hydraulic supply is linked to leaf photosynthetic capacity: evidence from New Caledonian and Tasmanian rainforests. *Plant, Cell & Environment* **23**: 1381–1388.

Brodribb TJ, Holbrook NM, Gutierrez M v. **2002**. Hydraulic and photosynthetic co-ordination in seasonally dry tropical forest trees. *Plant, Cell & Environment* **25**: 1435–1444.

Canadell JG, Monteiro PMS, Costa MH, Cunha LC da, Cox PM, Eliseev A v., Henson S, Ishii M, Jaccard S, Koven C, *et al.* 2021. Global carbon and other biogeochemical cycles and feedbacks. In: Climate Change 2021: The Physical Science Basis. Contribution of Working Group I to the Sixth Assessment Report of the Intergovernmental Panel on Climate Change.

Cernusak LA, Hutley LB, Beringer J, Holtum JAM, Turner BL. **2011**. Photosynthetic physiology of eucalypts along a sub-continental rainfall gradient in northern Australia. *Agricultural and Forest Meteorology* **151**.

Chen J-W, Zhang Q, Cao K-F. **2008**. Inter-species variation of photosynthetic and xylem hydraulic traits in the deciduous and evergreen Euphorbiaceae tree species from a seasonally tropical forest in south-western China. *Ecological Research* **24**: 65.

Chiti T, Certini G, Grieco E, Valentini R. **2010**. The role of soil in storing carbon in tropical rainforests: The case of Ankasa Park, Ghana. *Plant and Soil* **331**: 453–461.

Choat B, Ball MC, Luly JG, Holtum JAM. **2005**. Hydraulic architecture of deciduous and evergreen dry rainforest tree species from north-eastern Australia. *Trees* **19**: 305–311.

Choat B, Jansen S, Brodribb TJ, Cochard H, Delzon S, Bhaskar R, Bucci SJ, Feild TS, Gleason SM, Hacke UG, *et al.* 2012. Global convergence in the vulnerability of forests to drought. *Nature 2012 491:7426* **491**: 752–755.

Cornelissen JHC, Lavorel S, Garnier E, Díaz S, Buchmann N, Gurvich DE, Reich PB, Ter Steege H, Morgan HD, Van Der Heijden MGA, *et al.* 2003. A handbook of protocols for standardised and easy measurement of plant functional traits worldwide. *Australian Journal of Botany* **51**.

Cornwell WK, Wright I, Turner J, Maire V, Barbour M, Cernusak L, Dawson T, Ellsworth D, Farquhar G, Griffiths H. **2016**. A global dataset of leaf delta 13C values. *Scientific Data*.

Cunningham SC. **2005**. Photosynthetic responses to vapour pressure deficit in temperate and tropical evergreen rainforest trees of Australia. *Oecologia* **142**: 521–528.

Demarez V, Duthoit S, Baret F, Weiss M, Dedieu G. **2008**. Estimation of leaf area and clumping indexes of crops with hemispherical photographs. *Agricultural and Forest Meteorology* **148**.

Domingues TF, Meir P, Feldpausch TR, Saiz G, Veenendaal EM, Schrodt F, Bird M, Djagbletey G, Hien F, Compaore H, *et al.* 2010. Co-limitation of photosynthetic capacity by nitrogen and phosphorus in West Africa woodlands. *Plant, Cell & Environment* **33**: 959–980.

Dong N, Prentice IC, Evans BJ, Caddy-Retalic S, Lowe AJ, Wright IJ, Colin Prentice I, Evans BJ, Caddy-Retalic S, Lowe AJ, *et al.* 2017. Leaf nitrogen from first principles: Field evidence for adaptive variation with climate. *Biogeosciences* **14**: 481–495.

Dong N, Prentice IC, Wright IJ, Evans BJ, Togashi HF, Caddy-Retalic S, McInerney FA, Sparrow B, Leitch E, Lowe AJ. **2020**. Components of leaf-trait variation along environmental gradients. *New Phytologist* **228**: 82–94.

Dong N, Prentice IC, Wright IJ, Wang H, Atkin OK, Bloomfield KJ, Domingues TF, Gleason SM, Maire V, Onoda Y, *et al.* 2022. Leaf nitrogen from the perspective of optimal plant function. *Journal of Ecology* **110**.

871 **Franklin O, Harrison SP, Dewar R, Farrior CE, Brännström Å, Dieckmann U, Pietsch S,**
872 **Falster D, Cramer W, Loreau M, *et al.* 2020**. Organizing principles for vegetation dynamics.
873 *Nature Plants* **6**: 444–453.

874 **Fu Z, Ciais P, Prentice IC, Gentine P, Makowski D, Bastos A, Luo X, Green JK, Stoy PC,**
875 **Yang H, *et al.* 2022**. Atmospheric dryness reduces photosynthesis along a large range of soil
876 water deficits. *Nature Communications 2022 13:1* **13**: 1–10.

877 **Gleason SM, Butler DW, Waryszak P**. **2013**. Shifts in leaf and stem hydraulic traits across
878 aridity gradients in eastern Australia. *International Journal of Plant Sciences* **174**: 1292–1301.

879 **Gleason SM, Butler DW, Ziemińska K, Waryszak P, Westoby M**. **2012**. Stem xylem
880 conductivity is key to plant water balance across Australian angiosperm species. *Functional*
881 *Ecology* **26**: 343–352.

882 **Gleason SM, Westoby M, Jansen S, Choat B, Hacke UG, Pratt RB, Bhaskar R, Brodribb**
883 **TJ, Bucci SJ, Cao KF, *et al.* 2016**. Weak tradeoff between xylem safety and xylem-specific
884 hydraulic efficiency across the world's woody plant species. *New Phytologist* **209**: 123–136.

885 **Granier A, Hue R, Barigah ST**. **1996**. Transpiration of natural rain forest and its dependence
886 on climatic factors. *Agricultural and Forest Meteorology* **78**: 19–29.

887 **Green JK, Berry J, Ciais P, Zhang Y, Gentine P**. **2020**. Amazon rainforest photosynthesis
888 increases in response to atmospheric dryness. *Science Advances* **6**.

889 **Grossiord C, Buckley TN, Cernusak LA, Novick KA, Poulter B, Siegwolf RTW, Sperry JS,**
890 **McDowell NG**. **2020a**. Plant responses to rising vapor pressure deficit. *New Phytologist* **226**:
891 1550–1566.

892 **Grossiord C, Ulrich DEM, Vilagrosa A**. **2020b**. Controls of the hydraulic safety–efficiency
893 trade-off. *Tree Physiology* **40**: 573–576.

894 **Gvozdevaite A**. **2018**. The role of economic, venation and morphological leaf traits in plant and
895 ecosystem function along forest-savanna gradients in the tropics.

Gvozdevaite A, Oliveras I, Domingues TF, Peprah T, Boakye M, Afriyie L, da Silva Peixoto K, de Farias J, Almeida de Oliveira E, Almeida Farias CC, *et al.* 2018. Leaf-level photosynthetic capacity dynamics in relation to soil and foliar nutrients along forest–savanna boundaries in Ghana and Brazil. *Tree Physiology* **38**: 1912–1925.

Hacke UG, Sperry JS, Pockman WT, Davis SD, McCulloh KA. **2001**. Trends in wood density and structure are linked to prevention of xylem implosion by negative pressure. *Oecologia 2000 126:4* **126**: 457–461.

Han T, Feng Q, Yu T, Yang X, Zhang X, Li K. **2022**. Characteristic of Stomatal Conductance and Optimal Stomatal Behaviour in an Arid Oasis of Northwestern China. *Sustainability 2022, Vol. 14, Page 968* **14**: 968.

Harrison SP, Cramer W, Franklin O, Prentice IC, Wang H, Brännström Å, de Boer H, Dieckmann U, Joshi J, Keenan TF, *et al.* 2021. Eco-evolutionary optimality as a means to improve vegetation and land-surface models. *New Phytologist* **231**: 2125–2141.

Hoeber S, Leuschner C, Köhler L, Arias-Aguilar D, Schuldt B. **2014**. The importance of hydraulic conductivity and wood density to growth performance in eight tree species from a tropical semi-dry climate. *Forest Ecology and Management* **330**: 126–136.

Hothorn T, Bretz F, Westfall P. **2008**. Simultaneous inference in general parametric models. *Biometrical Journal: Journal of Mathematical Methods in Biosciences* **50**: 346–363.

Hubau W, Lewis SL, Phillips OL, Affum-Baffoe K, Beeckman H, Cuní-Sanchez A, Daniels AK, Ewango CEN, Fauset S, Mukinzi JM. **2020**. Asynchronous carbon sink saturation in African and Amazonian tropical forests. *Nature* **579**: 80–87.

Jacobsen AL, Valdovinos-Ayala J, Pratt RB. **2018**. Functional lifespans of xylem vessels: Development, hydraulic function, and post-function of vessels in several species of woody plants. *American Journal of Botany* **105**.

Komsta L. **2011**. Package 'outliers'. *Medical University of Lublin, Lublin*.

Körner C. **2019**. No need for pipes when the well is dry—a comment on hydraulic failure in trees. *Tree Physiology* **39**.

Lê S, Josse J, Husson F. **2008**. FactoMineR: an R package for multivariate analysis. *Journal of statistical software* **25**: 1–18.

Liu H, Gleason SM, Hao G, Hua L, He P, Goldstein G, Ye Q. **2019**. Hydraulic traits are coordinated with maximum plant height at the global scale. *Science Advances* **5**: eaav1332.

Liu L, Gudmundsson L, Hauser M, Qin D, Li S, Seneviratne SI. **2020**. Soil moisture dominates dryness stress on ecosystem production globally. *Nature Communications* **11**: 4892.

Liu H, Ye Q, Gleason SM, He P, Yin D. **2021**. Weak tradeoff between xylem hydraulic efficiency and safety: climatic seasonality matters. *New Phytologist* **229**: 1440–1452.

López R, Cano FJ, Martin-Stpaul NK, Cochard H, Choat B. **2021**. Coordination of stem and leaf traits define different strategies to regulate water loss and tolerance ranges to aridity. *New Phytologist* **230**: 497–509.

Madansky A, Alexander H. **2017**. Weighted standard error and its impact on significance testing. *The Analytical Group, Inc*.

Maire V, Martre P, Kattge J, Gastal F, Esser G, Fontaine S, Soussana J-F. **2012**. The coordination of leaf photosynthesis links C and N fluxes in C3 plant species. *PloS one* **7**: e38345.

Maire V, Wright IJ, Prentice IC, Batjes NH, Bhaskar R, van Bodegom PM, Cornwell WK, Ellsworth D, Niinemets Ü, Ordonez A. **2015**. Global effects of soil and climate on leaf photosynthetic traits and rates. *Global Ecology and Biogeography* **24**: 706–717.

Malhi Y, Girardin C, Metcalfe DB, Doughty CE, Aragão LEOC, Rifai SW, Oliveras I, Shenkin A, Aguirre-Gutiérrez J, Dahlsjö CAL, *et al.* 2021. The Global Ecosystems Monitoring network: Monitoring ecosystem productivity and carbon cycling across the tropics. *Biological Conservation* **253**: 108889.

Manzoni S, Vico G, Katul G, Palmroth S, Jackson RB, Porporato A. **2013**. Hydraulic limits on maximum plant transpiration and the emergence of the safety–efficiency trade-off. *New Phytologist* **198**: 169–178.

Martínez-Vilalta J, Cochard H, Mencuccini M, Sterck F, Herrero A, Korhonen JFJ, Llorens P, Nikinmaa E, Nolè A, Poyatos R, *et al.* 2009. Hydraulic adjustment of Scots pine across Europe. *The New phytologist* **184**: 353–364.

Medlyn BE, Duursma RA, Eamus D, Ellsworth DS, Prentice IC, Barton CVM, Crous KY, de Angelis P, Freeman M, Wingate L. **2011**. Reconciling the optimal and empirical approaches to modelling stomatal conductance. *Global Change Biology* **17**: 2134–2144.

Mencuccini M, Manzoni S, Christoffersen B. **2019a**. Modelling water fluxes in plants: from tissues to biosphere. *New Phytologist* **222**: 1207–1222.

Mencuccini M, Rosas T, Rowland L, Choat B, Cornelissen H, Jansen S, Kramer K, Lapenis A, Manzoni S, Niinemets Ü, *et al.* 2019b. Leaf economics and plant hydraulics drive leaf : wood area ratios. *New Phytologist* **224**: 1544–1556.

Moore S, Adu-Bredu S, Duah-Gyamfi A, Addo-Danso SD, Ibrahim F, Mbou AT, de Grandcourt A, Valentini R, Nicolini G, Djagbletey G, *et al.* 2018. Forest biomass, productivity and carbon cycling along a rainfall gradient in West Africa. *Global Change Biology* **24**: e496–e510.

Neelin JD, Münnich M, Su H, Meyerson JE, Holloway CE. **2006**. Tropical drying trends in global warming models and observations. *Proceedings of the National Academy of Sciences* **103**: 6110–6115.

Niinemets Ü, Wright IJ, Evans JR. **2009**. Leaf mesophyll diffusion conductance in 35 Australian sclerophylls covering a broad range of foliage structural and physiological variation. *Journal of Experimental Botany* **60**: 2433–2449.

Ögren E. **1993**. Convexity of the Photosynthetic Light-Response Curve in Relation to Intensity and Direction of Light during Growth. *Plant physiology* **101**: 1013–1019.

Oliveras I, Bentley L, Fyllas NM, Gvozdevaite A, Shenkin AF, Peprah T, Morandi P, Peixoto KS, Boakye M, Adu-Bredu S, *et al.* 2020. The Influence of Taxonomy and Environment on Leaf Trait Variation Along Tropical Abiotic Gradients. *Frontiers in Forests and Global Change* **3**: 18.

Olson ME, Anfodillo T, Rosell JA, Petit G, Crivellaro A, Isnard S, León-Gómez C, Alvarado-Cárdenas LO, Castorena M. **2014**. Universal hydraulics of the flowering plants: vessel diameter scales with stem length across angiosperm lineages, habits and climates. *Ecology Letters* **17**: 988–997.

Olson ME, Rosell JA. **2013**. Vessel diameter–stem diameter scaling across woody angiosperms and the ecological causes of xylem vessel diameter variation. *New Phytologist* **197**: 1204–1213.

Peng Y, Bloomfield KJ, Cernusak LA, Domingues TF, Colin Prentice I. **2021**. Global climate and nutrient controls of photosynthetic capacity. *Communications Biology 2021 4:1* **4**: 1–9.

Peng Y, Bloomfield KJ, Prentice IC. **2020**. A theory of plant function helps to explain leaf-trait and productivity responses to elevation. *New Phytologist* **226**: 1274–1284.

Pfautsch S, Harbusch M, Wesolowski A, Smith R, Macfarlane C, Tjoelker MG, Reich PB, Adams MA. **2016**. Climate determines vascular traits in the ecologically diverse genus Eucalyptus. *Ecology Letters* **19**: 240–248.

Poorter L, McDonald I, Alarcón A, Fichtler E, Licona JC, Peña-Claros M, Sterck F, Villegas Z, Sass-Klaassen U. **2010**. The importance of wood traits and hydraulic conductance for the performance and life history strategies of 42 rainforest tree species. *New Phytologist*.

Prentice IC, Dong N, Gleason SM, Maire V, Wright IJ. **2014**. Balancing the costs of carbon gain and water transport: testing a new theoretical framework for plant functional ecology. *Ecology Letters* **17**: 82–91.

Pritzkow C, Williamson V, Szota C, Trouvé R, Arndt SK. **2020**. Phenotypic plasticity and genetic adaptation of functional traits influences intra-specific variation in hydraulic efficiency and safety. *Tree Physiology* **40**: 215–229.

Quesada CA, Lloyd J, Schwarz M, Patiño S, Baker TR, Czimczik C, Fyllas NM, Martinelli L, Nardoto GB, Schmerler J, *et al.* 2010. Variations in chemical and physical properties of Amazon forest soils in relation to their genesis. *Biogeosciences* **7**.

Raab N. **2020**. Non-structural carbohydrates and leaf ecophysiology in tropical and temperate forests.

Restrepo-Coupe N, da Rocha HR, Hutyra LR, da Araujo AC, Borma LS, Christoffersen B, Cabral OMR, de Camargo PB, Cardoso FL, da Costa ACL, *et al.* 2013. What drives the seasonality of photosynthesis across the Amazon basin? A cross-site analysis of eddy flux tower measurements from the Brasil flux network. *Agricultural and Forest Meteorology* **182–183**: 128–144.

Rodriguez-Dominguez CM, Brodribb TJ. **2020**. Declining root water transport drives stomatal closure in olive under moderate water stress. *New Phytologist* **225**.

Rogers A, Medlyn BE, Dukes JS, Bonan G, von Caemmerer S, Dietze MC, Kattge J, Leakey ADB, Mercado LM, Niinemets Ü, *et al.* 2017. A roadmap for improving the representation of photosynthesis in Earth system models. *New Phytologist* **213**: 22–42.

Ryan MG, Yoder BJ. **1997**. Hydraulic Limits to Tree Height and Tree Growth. *BioScience* **47**.

Sandoval D, Prentice IC. **2020**. Simple process-led algorithms for simulating habitats (SPLASH v.2.0): robust calculations of water and energy fluxes in complex terrain. *EGU General Assembly 2020* .

Santiago LS, Goldstein G, Meinzer FC, Fisher JB, Machado K, Woodruff D, Jones T. **2004**. Leaf photosynthetic traits scale with hydraulic conductivity and wood density in Panamanian forest canopy trees. *Oecologia* **140**: 543–550.

Schuldt B, Leuschner C, Brock N, Horna V. **2013**. Changes in wood density, wood anatomy and hydraulic properties of the xylem along the root-to-shoot flow path in tropical rainforest trees. *Tree physiology* **33**: 161–174.

Smith NG, Keenan TF, Prentice IC, Wang H, Wright IJ, Niinemets U, Crous KY, Domingues TF, Guerrieri R, Ishida FY, *et al.* 2019. Global photosynthetic capacity is optimized to the environment.

Sperry JS, Hacke UG, Oren R, Comstock JP. **2002**. Water deficits and hydraulic limits to leaf water supply. *Plant, Cell & Environment* **25**: 251–263.

Sperry JS, Venturas MD, Anderegg WRL, Mencuccini M, Mackay DS, Wang Y, Love DM. **2017**. Predicting stomatal responses to the environment from the optimization of photosynthetic gain and hydraulic cost. *Plant Cell and Environment* **40**.

Stangl ZR, Tarvainen L, Wallin G, Ubierna N, Räntfors M, Marshall JD. **2019**. Diurnal variation in mesophyll conductance and its influence on modelled water-use efficiency in a mature boreal Pinus sylvestris stand. *Photosynthesis Research* **141**: 53–63.

Stocker BD, Wang H, Smith NG, Harrison SP, Keenan TF, Sandoval D, Davis T, Prentice IC. **2020**. P-model v1.0: An optimality-based light use efficiency model for simulating ecosystem gross primary production. *Geoscientific Model Development* **13**: 1545–1581.

Togashi HF, Prentice IC, Evans BJ, Forrester DI, Drake P, Feikema P, Brooksbank K, Eamus D, Taylor D. **2015**. Morphological and moisture availability controls of the leaf area-to-sapwood area ratio: analysis of measurements on A ustralian trees. *Ecology and Evolution* **5**: 1263–1270.

Walker AP, Beckerman AP, Gu L, Kattge J, Cernusak LA, Domingues TF, Scales JC, Wohlfahrt G, Wullschleger SD, Woodward FI. **2014**. The relationship of leaf photosynthetic traits – Vcmax and Jmax – to leaf nitrogen, leaf phosphorus, and specific leaf area: a meta-analysis and modeling study. *Ecology and Evolution* **4**: 3218–3235.

Wang H, Prentice IC, Davis TW, Keenan TF, Wright IJ, Peng C. **2017a**. Photosynthetic responses to altitude: an explanation based on optimality principles. *New Phytologist* **213**: 976–982.

Wang H, Prentice IC, Keenan TF, Davis TW, Wright IJ, Cornwell WK, Evans BJ, Peng C. **2017b**. Towards a universal model for carbon dioxide uptake by plants. *Nature Plants 2017 3:9* **3**: 734–741.

Warton DI, Duursma RA, Falster DS, Taskinen S. **2012**. smatr 3-an R package for estimation and inference about allometric lines. *Methods in ecology and evolution* **3**: 257–259.

Wright IJ, Reich PB, Cornelissen JHC, Falster DS, Groom PK, Hikosaka K, Lee W, Lusk CH, Niinemets Ü, Oleksyn J. **2005**. Modulation of leaf economic traits and trait relationships by climate. *Global Ecology and Biogeography* **14**: 411–421.

Wright IJ, Reich PB, Westoby M. **2001**. Strategy shifts in leaf physiology, structure and nutrient content between species of high- and low-rainfall and high- and low-nutrient habitats. *Functional Ecology* **15**: 423–434.

Wright IJ, Reich PB, Westoby M. **2003**. Least-cost input mixtures of water and nitrogen for photosynthesis. *The American naturalist* **161**: 98–111.

Wright IJ, Reich PB, Westoby M, Ackerly DD, Baruch Z, Bongers F, Cavender-Bares J, Chapin T, Cornellssen JHC, Diemer M, *et al.* 2004. The worldwide leaf economics spectrum. *Nature 2004 428:6985* **428**: 821–827.

Wu J, Serbin SP, Ely KS, Wolfe BT, Dickman LT, Grossiord C, Michaletz ST, Collins AD, Detto M, McDowell NG, *et al.* 2020. The response of stomatal conductance to seasonal drought in tropical forests. *Global Change Biology* **26**: 823–839.

Xu H, Wang H, Prentice IC, Harrison SP, Wright IJ. **2021**. Coordination of plant hydraulic and photosynthetic traits: confronting optimality theory with field measurements. *New Phytologist* **232**: 1286–1296.

Yamazaki D, Ikeshima D, Sosa J, Bates PD, Allen GH, Pavelsky TM. **2019**. MERIT Hydro: A high-resolution global hydrography map based on latest topography dataset. *Water Resources Research* **55**: 5053–5073.

Yang J, He Y, Aubrey DP, Zhuang Q, Teskey RO. **2016**. Global patterns and predictors of stem CO2 efflux in forest ecosystems. *Global Change Biology* **22**: 1433–1444.

Yang Y, Wang H, Harrison SP, Prentice IC, Wright IJ, Peng C, Lin G. **2019**. Quantifying leaf-trait covariation and its controls across climates and biomes. *New Phytologist* **221**: 155–168.

Zanne AE, Lopez-Gonzalez G, Coomes DA, Ilic J, Jansen S, Lewis SL, Miller RB, Swenson NG, Wiemann MC, Chave J. **2009**. Data from: Towards a worldwide wood economics spectrum.

Zhang Y, Chen JM, Miller JR. **2005**. Determining digital hemispherical photograph exposure for leaf area index estimation. In: Agricultural and Forest Meteorology.